Acta Biomaterialia 173 (2024) 261–282

Contents lists available at ScienceDirect

Acta Biomaterialia

journal homepage: www.elsevier.com/locate/actbio

Full length article

Implantable SDF-1α-loaded silk fibroin hyaluronic acid aerogel sponges as an instructive component of the glioblastoma ecosystem: Between chemoattraction and tumor shaping into resection cavities

Rodolfo Molina-Peña[a,1], Natália Helen Ferreira[a,1], Charlotte Roy[a], Loris Roncali[a], Mathie Najberg[a], Sylvie Avril[a], Mariana Zarur[b], William Bourgeois[c], Alba Ferreirós[g], Chiara Lucchi[e], Francesco Cavallieri[d], François Hindré[a], Giovani Tosi[f], Giuseppe Biagini[e], Franco Valzania[d], François Berger[c], Miguel Abal[g], Audrey Rousseau[a], Frank Boury[a], Carmen Alvarez-Lorenzo[b,1,*], Emmanuel Garcion[a,1,*]

[a] *Univ Angers, Nantes Université, Inserm, CNRS, CRCI2NA, SFR ICAT, F-49000 Angers, France*
[b] *Departamento de Farmacología, Farmacia y Tecnología Farmacéutica, ID Farma (GI-1645), Facultad de Farmacia, iMATUS, and Health Research Institute of Santiago de Compostela (IDIS), Universidade de Santiago de Compostela, 15782 Santiago de Compostela, Spain*
[c] *Inserm UMR1205, Brain Tech Lab, Grenoble Alpes University Hospital (CHUGA), Grenoble, 38000, France*
[d] *Neurology Unit, Neuromotor and Rehabilitation Department, Azienda USL-IRCCS di Reggio Emilia, Reggio Emilia, Italy*
[e] *Department of Biomedical, Metabolic and Neural Sciences, University of Modena and Reggio Emilia, 41125 Modena, Italy*
[f] *Department of Life Sciences, University of Modena and Reggio Emilia, 41125 Modena, Italy*
[g] *NASASBIOTECH S.L., Cantón Grande nº 9, 15003, A Coruña, Spain*

ARTICLE INFO

Article history:
Received 25 May 2023
Revised 16 October 2023
Accepted 17 October 2023
Available online 20 October 2023

Keywords:
Resection cavity
Implantable device
Cancer cell trap
Chemoattraction
Ecosystem dynamic
Cell homing

ABSTRACT

In view of inevitable recurrences despite resection, glioblastoma (GB) is still an unmet clinical need. Dealing with the stromal-cell derived factor 1-alpha (SDF-1α)/CXCR4 axis as a hallmark of infiltrative GB tumors and with the resection cavity situation, the present study described the effects and relevance of a new engineered micro-nanostructured SF-HA-Hep aerogel sponges, made of silk fibroin (SF), hyaluronic acid (HA) and heparin (Hep) and loaded with SDF-1α, to interfere with the GB ecosystem and residual GB cells, attracting and confining them in a controlled area before elimination. 70 µm-pore sponges were designed as an implantable scaffold to trap GB cells. They presented shape memory and fit brain cavities. Histological results after implantation in brain immunocompetent Fischer rats revealed that SF-HA-Hep sponges are well tolerated for more than 3 months while moderately and reversibly colonized by immuno-inflammatory cells. The use of human U87MG GB cells overexpressing the CXCR4 receptor (U87MG-CXCR4+) and responding to SDF-1α allowed demonstrating directional GB cell attraction and colonization of the device *in vitro* and *in vivo* in orthotopic resection cavities in Nude rats. Not modifying global survival, aerogel sponge implantation strongly shaped U87MG-CXCR4+ tumors in cavities in contrast to random infiltrative growth in controls. Overall, those results support the interest of SF-HA-Hep sponges as modifiers of the GB ecosystem dynamics acting as "cell meeting rooms" and biocompatible niches whose properties deserve to be considered toward the development of new clinical procedures.

Statement of Significance

Brain tumor glioblastoma (GB) is one of the worst unmet clinical needs. To prevent the relapse in the resection cavity situation, new implantable biopolymer aerogel sponges loaded with a chemoattractant molecule were designed and preclinically tested as a prototype targeting the interaction between the initial tumor location and its attraction by the peritumoral environment. While not modifying global survival, biocompatible SDF1-loaded hyaluronic acid and silk fibroin sponges induce directional GB cell

* Corresponding authors.
E-mail addresses: carmen.alvarez.lorenzo@usc.es (C. Alvarez-Lorenzo), emmanuel.garcion@univ-angers.fr (E. Garcion).
[1] Eq contribution.

https://doi.org/10.1016/j.actbio.2023.10.022

attraction and colonization *in vitro* and in rats *in vivo*. Interestingly, they strongly shaped GB tumors in contrast to random infiltrative growth in controls. These results provide original findings on application of exogenous engineered niches that shape tumors and serve as cell meeting rooms for further clinical developments.

1. Introduction

Glioblastoma (GB) is a lethal tumor with high recurrence rates. Most recurrences occur within 2 cm of the resection cavity due to the infiltration of GB cells into the brain parenchyma [1–3]. Targeting residual tumor cells is crucial to improve patient outcomes. New strategies are needed to selectively kill these cells while minimizing damage to normal brain tissue.

In contrast to direct targeting strategies that vectorize killing agents toward cancer cells, the reversal approach involves bringing the target toward a site of confinement by mimicking the preferred environment of infiltrating tumor cells [4,5]. Then, direct loco-regional delivery of a cell death signal, such as focalized radiotherapy or local delivery of cytotoxic chemotherapeutic agents, could be applied for more effective treatment.

The tumor cell trapping strategy has been applied by a few groups like De la Fuente et al. who designed a polyurethane scaffold coated with collagen that was able to confine metastatic ovarian cancer cells in mice peritonea showing an improvement in survival [6]. Jain et al. designed aligned fibers of polycaprolactone to direct GB cells toward an extracortical killing sink [7]. Reduced tumor size was observed; however, the invasive behavior of GB cells did not allow for a complete recovery. More research in this area shall be beneficial for the development of more effective glioblastoma treatment.

For this purpose, biocompatible biomaterials that can support cell infiltration should be chosen [8,9]. The scaffold should be biomimetically functionalized to adapt its structure and composition, including relevant extracellular matrix (ECM) components, such as hyaluronic acid (HA), which is a crucial element of the cerebral ECM [10,11]. Also, an active scaffold can contain specific cellular signals that respond to the desired application, such as a chemokine to increase the recruitment of cancer cells.

In this regard, it has been observed that infiltrative GB cells express the C-X-C chemokine receptor type 4 (CXCR4) [12–14]. This receptor binds the chemoattractant stromal cell-derived factor 1 α (SDF-1α), also known as CXCL12. A gradient of this chemokine induces the attraction of cells expressing the CXCR4 receptor [15,16]. Therefore, we hypothesize that implanting a scaffold containing SDF-1α in the resection cavity can attract and confine infiltrative GB cells into a specific site.

Previously, our group developed freeze-dried aerogel sponges for this purpose: a silk fibroin (SF) with Hyaluronic acid (HA) sponge (SF-HA), and a SF with HA and heparin (Hep) (SF-HA-Hep) sponge, where heparin acts as a complexation agent for SDF-1α [17]. This study aims to evaluate the capacity of this new scaffold to attract infiltrative GB cells in a rat model of the brain resection cavity.

The biocompatibility and biodegradability of sponges were first evaluated. Direct placement of GB cells and glioma spheroids in contact with the scaffolds was used to evaluate cellular interactions and their cell hosting capacity. SF-HA-Hep sponges were selected for further application based on their degradation profile and enhanced cell adhesion. Our results showed that SDF-1α-loaded sponges had a strong *in vitro* chemotactic response and enhanced colonization. *In vivo* assessment was conducted by the placement of sponges 1-mm away to human GB cells expressing the CXCR4 receptor. Sponges attracted GB cells and induced localized tumor development in the resection spaces, which can be potentially used for further focalized therapy in a concentrated area. The findings and limitations of this strategy are discussed for further development of a safer and more efficient GB cell confinement device.

2. Materials and methods

2.1. Materials

Hepes, bovine serum albumin (BSA), resazurin, paraformaldehyde (PFA), sucrose, low melting point low gelling temperature agarose, Sudan Black, Giemsa stain, Crystal violet, Phosphate Buffered Saline (PBS, pH 7.4), Dulbecco′s Modified Eagle′s Medium (DMEM) with high glucose and Aphidicolin (ADC) were purchased from Sigma-Aldrich; glycerol (86–89 wt%) from Fluka and heparin sodium salt (Mw 15,000 ± 2000 g/mol) from Calbiochem (Billerca MA, USA), N-(3-dimethylaminopropyl)-N′-ethylcarbodiimide hydrochloride (EDC) and N-hydroxysulfosuccinimide sodium salt (NHS) from Acros Organics (New Jersey, USA). Hyaluronic acid (HA) (Mw 360,000 g/mol) was purchased from Guinama (Valencia, Spain). Silk fibroin (SF) 8 wt% in an aqueous solution was provided by IMIDA (Murcia, Spain). SDF-1α was purchased from Miltenyi Biotec (Paris, France).

2.1.1. Sponges' preparation and characterization

SF (4 %) with HA (2 %) (SF-HA) and SF (4 %) with HA (2 %) and heparin (1 %) (SF-HA-hep) sponges were synthesized and physicochemically characterized as reported previously by Najberg et al. (2020) [17]. Briefly, HA was dissolved in Hepes buffer ($C_{Hepes} = 20.10^{-3}$ M, $C_{NaCl} = 0.15$ M, pH=7.4) to obtain a final concentration of 4% w/v. SF 8% w/v solution was gently mixed with an equivalent volume of HA 4 % solution in Hepes buffer with or without heparin sodium salt ($C_f = 1\%$ w/v). The SF-HA mixture was crosslinked using 5 mg/mL EDC and 1.8 mg/mL NHS. For formulations with heparin, 15 mg/mL EDC and 5.5 mg/mL NHS were used. The solutions were poured into a 96-well plate, covered, and allowed to crosslink for 15 h at 4 °C. The gels were then frozen at −20 °C for 24 h and freeze-dried in a Telstar® LyoQuest at −70 °C and 0.01 mBar overnight. The stabilization occurred by annealing the sponges in ethanol vapors, followed by freeze-drying again.

The porosity, thickness, and pore size of the sponges (n = 3) were evaluated by microcomputed tomography (microCT) using a Bruker SkyScan 1272 (Kontich, Belgium). Scans were acquired at a voltage of 50 kV and a current of 200 μA, with a rotation step of 0.3°, pixel size of 5 μm, and no filter. Reconstruction of the obtained tomograms was carried out using NRecon software (Bruker) and 3D rendered images of the samples were generated through original volumetric reconstructed images by CTVox (Bruker). The quantification of structure properties was evaluated using a cylindric volume of interest (VOI) of 30 mm^3 centered in the middle of the samples. Before the analysis, datasets were binarized using

a global threshold of 70–255 and a 3D despeckle process was applied to reduce image noise. Finally, analysis was performed using CTAn software (Bruker).

Sponges, measuring 2 mm - height and 3 mm - diameter, underwent sterilization under UV light for 30 min on each side prior to both *in vitro* and *in vivo* procedures.

2.1.2. Cell lines and culture conditions

NIH3T3 mouse fibroblast cells (CRL-1658™) and U87-MG cells were acquired from ATCC (Rockville, Maryland, USA). U87-MG cells, transduced to express the CXCR4 receptor and red fluorescent protein (RFP) as previously described [18]. Transduced cells were selected with Blasticidine treatment (10 µg/mL) followed by cell sorting of a pure subpopulation expressing RFP and the CXCR4 receptor. These cells were called here as U87MG-CXCR4$^+$. All cell lines were cultured at 37 °C and 5 % CO_2 in DMEM supplemented with 10 % fetal bovine serum (FBS) and 1 % penicillin/streptomycin and subcultured every 3.5 days.

2.2. In vitro methods

2.2.1. Flow cytometry

U87MG-CXCR4+ cells were dissociated with trypsin, washed and incubated with 10 μg/mL anti-CXCR4 primary antibody clone 12G5, or IgG2a [18] in PBS containing 0.5 % BSA for 40 min at 4 °C. After washing with PBS/BSA, cells were incubated with 8 µg/mL secondary Ab (Polyclonal goat α-mouse IGs-FITC, Dako F0479) in PBS containing 0.5 % BSA for 30 min at 4 °C protected from light. After washing in PBS/BSA cells were analyzed in a MACSQuant® Analyzer 10 Flow Cytometer (Miltenyi Biotec).

2.2.2. Western blot

Total proteins were isolated from U87MG-CXCR4+ cells by sonication in a lysis buffer composed of 50 mM HEPES, pH 7.5, 150 mM NaCl, 1 mM EDTA, pH 8, 2.5 mM EGTA, pH 7.4, 0.1 % Tween 20, 10 % glycerol, 0.1 mM sodium orthovanadate, 1 mM sodium fluoride, 10 mM glycerophosphate and 0.1 mM phenylmethylsulphonyl fluoride (PMSF). After quantification by spectrophotometry using the Quick Start™ Bradford Protein Assay (Bio-rad), equal amounts of proteins (20 µg) were loaded onto 10 % polyacrylamide gels and transferred to an Amersham GE Healthcare nitrocellulose membrane (0.45 μm pore size; Fisher Scientific). The following antibodies were used according to the manufacturer's instructions: rabbit anti-human Akt (Cell Signaling, #9272), phosphor-Akt (Ser473; #9271), p44/42 MAPK Erk1/2 (#9102), phospho-p44/42 MAPK Erk1/2 (Thr202/Tyr204; #9101), paxillin (#2542), and phosphor-paxillin (Tyr118; #2541). A mouse anti-human actin (#MA5–11,869, Invitrogen) was used as a loading control. Anti-Rabbit IgG Secondary Antibody, HRP conjugate (Fisher Scientific) was used at a dilution of 1:10,000. Detection was performed on SuperSignal™ West Femto Maximum Sensitivity Substrate (Fisher Scientific) with a ChemiCapt 3000 imaging system (Vilber Lourmat, Marne-la-Vallée France).

2.2.3. Viability assay

The cytotoxicity of sponges on NIH3T3 and U87MG cells was evaluated by the indirect and direct contact methods, by ISO 10,993–5:2009, at 24 h and 72 h intervals. 4×10^4 NIH3T3 cells were seeded per well (24-well plates) for the 24-h assay and 1×10^4 cells/well for the 72-h assay. 8×10^4 U87MG cells were seeded per well for the 24-h assay and 2×10^4 cells/well for the 72-h assay. Cells were kept at 37 °C and 5 % CO_2 for 24 h before adding the sponges. UV-sterilized 2 mm height and 3 mm diameter sponges were washed 3 times with PBS, for residual crosslinker removal, and equilibrated in complete medium before use. For the direct contact method, sponges were directly added on top of the cell monolayer. Wells without sponges were used as controls. 24 h or 72 h after, sponges were removed by aspiration, and the media was replaced with 500 µL of 44 µM resazurin. After 2 h, cell viability was estimated by the fluorescence intensity of the resorufin (545–600 nm) using the ClarioStar microplate fluorometer (BMG Labtech GmbH, Ortenberg, Germany). For the indirect contact method, suspended culture inserts with the sponges inside (MilliCell, PET, 8 µm) were placed in the wells containing cells. Inserts without sponges were used as controls. 200 µL of media was added to completely cover the sponges. The viability of the cells was measured as described above. Triplicates were performed for all used conditions.

2.2.4. Agarose drop assay

The ability of SDF-1α (Miltenyi Biotec) to induce the migration of U87MG-CXCR4+ cells was evaluated using an adapted agarose drop assay [19]. Briefly, a 24-well plate was coated with the extracellular matrix from U87MG cells. To do so, wells were first coated with poly-d-lysine (PDL, Sigma), then 5×10^4 U87MG cells were cultured for 48 h, lysed with deionized water, washed with PBS, and air-dried under sterile conditions before use. Then, a 2 µL drop of 1% w/v agarose in PBS containing 1×10^5 cells was placed in the center of a well. The agarose was allowed to solidify at 4 °C for 10 min. Then, 500 µL of serum-free DMEM with or without the chemokine (40 ng/mL of SDF-1α), and with or without 20 µg/mL aphidicolin (ADC) acting as an inhibitor of proliferation, was added on top of the drops. Plates were incubated for 3 days at 37 °C and 5 % CO_2. The distance of migration was measured at 4 points of the drop between the edge of the drop and the front of migration with ImageJ.

2.2.5. Boyden chamber assay

U87MG-CXCR4$^+$cells were starved in serum-free DMEM (SFM) for 24 h. Then cells were collected with Acutase solution, washed with PBS and resuspended in SFM. 5×10^4 cells were deposited on top of 8-µm pore PET inserts (Corning 353,097) in 100 µL of SFM. Then, 650 µL of SF DMEM containing 0, 40 or 120 ng/mL SDF-1α was deposited in the bottom well. After 18-h incubation cells were fixed with 4 % PFA for 15 min at room temperature (RT) and stained with 0.1 % crystal violet solution for 30 min. After washing, images were obtained in a VHX-7000 microscope (Keyence, France), and cells were counted with the QuPath software.

2.2.6. U87MG cells interaction with sponges

The cell response of U87MG cells when cultured into the sponges matrix was evaluated by direct seeding of cells into the sponges. SF-HA and SF-HA-Hep (1 % heparin) sponges were hydrated and cut in 2-mm height cylinders. After washing in PBS, they were sterilized by 30-min UV cycles each side. Sponges were washed with PBS and equilibrated in complete DMEM medium (10 % FBS and 1 % antibiotics). The excess medium was blotted in sterile gauzes for 20 s on each side. The sponges were then transferred to individual wells (24-well plate) and a drop containing 5×10^4 cells in 20 µL of medium was slowly deposited on top of the sponges. Sponges with cells were left for 30 min in the incubator to allow for cell adherence. Following this, 500 µL of complete DMEM was added and the sponges incubated for 2 days at 37 °C and 5 % CO_2. Revelation of the cellular response was performed by replacing the medium with complete DMEM containing 44 mM resazurin followed by incubation for 3 h. Controls well consisted in the same number of cells cultured on plastic.

The adherence and spreading of U87MG cells in SF-HA and SF-HA-Hep sponges were observed using a scanning electron microscope (SEM) Evo LS15 (Zeiss, USA). 60 µL DMEM containing 1×10^5 U87MG cells was deposited onto a 2-mm height sponge and cells were allowed to adhere for 1 h before the addition of

500 µL of complete DMEM in a 24-well plate. Constructs were cultured for 3 days at 37 °C and 5 % CO_2. 2.5 % glutaraldehyde in 0.1 M phosphate buffer was used for fixation for 2 h. After PBS and distilled water rinsing (1x for 5 min), constructs were incubated in 1 % osmium tetroxide aqueous solution for 1 h at RT. The samples were cut in half then rinsed with distilled water (3x for 5 min), followed by dehydration performed in increasing concentrations of ethanol solutions 50, 70, and 95 % for 20 min each, and 100 %, (3x for 30 min). Desiccation was performed in ethanol:hexamethyldisilazane (HDMS) 1:1 for 45 min, and HDMS overnight. A platinum coating was performed before the analysis of the surface and transverse sections of the different sponges.

2.2.7. Under agarose cell migration assay

The assay was adapted from Heit and Kubes, 2003 [20]. Agarose was dissolved in PBS by microwave heating and mixed with serum-free DMEM at 70 °C. The resulting mixture containing 1.2 % agarose in 75 % DMEM was sterile-filtered and equilibrated for 15 min at 37 °C before depositing 3 mL into each well of a 6-well plate. Casted gels were left to solidify for 30 min at RT and 1 h at 4 °C. Three punches were made in each gel using a homemade template and a 4-mm biopsy punch. The cut agarose was aspirated to create three reservoirs separated by equal distances of 2 mm. 5×10^4 U87MG-CXCR4+ cells previously treated with 1 µg/mL of ADC for 24 h in complete medium were seeded in 20 µL of DMEM containing either 1 % FBS or 10 % FBS, and 5 µg/mL of ADC, in the center well. Sterile sponges loaded with either 10 pmol or 100 pmol of SDF-1α were deposited in the right chamber and covered with 15 uL of serum-free DMEM. PBS was put in the left compartment acting as a control. To assess the effect of sponges without SDF-1α, the latter were evaluated against only PBS that was deposited in the left compartment. The comparison of the cell migration response to sponges loaded with SDF-1α (100 pmol) vs sponges alone was also carried out by placement of the former in the right wells and the sponges alone in the left well. After 3 days of incubation, the constructs were fixed with a mixture of methanol and acetic acid (3:1) and after removal of the gels, cells were stained with Giemsa stain (1:10), and washed 3x with distilled water. Pictures were taken with a VHX-7000 digital microscope (Keyence, France) and the areas of migration from the edge of the center well toward the left and right flanks were quantified with ImageJ.

2.2.8. Glioma spheroids assay

U87MG-CXCR4+ cells were cultured at a density of 6000 cells/cm^2 in defined medium consisting of a 1:1 mixture of low glucose DMEM and Ham's F12 supplemented with 20 ng/mL EGF and FGF-2, 5 µg/mL heparin, 1x B27 supplement and 1 % v/v Penicillin/Streptomycin. Half of the medium was changed every 3.5 days and spheroids were subcultured every 7 days. A single D7-neurospheroid of around 200 µm was collected and deposited on top of a 2-mm height and 6-mm diameter UV-sterilized sponge that was previously loaded with 60 µL serum-free DMEM containing 100 pmol of SDF-1α. Sponges without SDF-1α were used as controls. After 1-h of incubation at 37 °C and 5 % CO_2, 400 µL of DMEM supplemented with 1 % FBS, 1 % N1, and 1 % antibiotics was added carefully into the well (24 well plate). The constructs were left in culture for 6 days, fixed with 4 % PFA, permeabilized, and stained with DAPI before incubation in 0.3 % Soudan Black solubilized in 70 % ethanol to reduce the autofluorescence of sponges. Confocal images were obtained from the top view and the cross-section of sliced constructs. The on-top cell area and the cross-section invaded area were analyzed with the QuPath software.

2.3. In vivo studies

2.3.1. Animals

Fischer and nude athymic female rats aged 8–10 weeks were obtained from Janvier Labs (Le Genest-Saint-Isle, France). The protocol was approved by the Ethical Committee for Animal Experimentation of Pays de la Loire region, France (authorization number APAFIS #25889-2020032620074335 v3).

2.3.2. Evaluation of the biocompatibility of sponges

2.3.2.1. Implantation of sponges. Fisher rats were anesthetized by intraperitoneal injection of a mixture of ketamine (80 mg/kg) and xylazine (10 mg/kg) with subcutaneous administration of ketoprofen (5 mg/Kg) and positioned in a Kopf stereotaxic instrument. A 10 mm-long incision was made along the midline to create access to the surface of the skull. Following this, a burr hole (stereotactic coordinates: P: +0.8 mm; L: −3 mm (right from the bregma)) was drilled into the skull using a high-speed drill to expose the brain tissues underneath. A portion of the brain cortex was then carefully cut using a biopsy punch device and subsequently removed using vacuum suction to create a cavity that was approximately 3 mm wide and 2 mm deep. SF-HA and SF-HA-hep sponges were swollen in PBS, cut transversely to obtain 2 mm height cylinders, and sterilized under UV light for 1 hour. The sponges were then cut one by one before implantation with a 3 mm diameter biopsy punch with a push-button and, immediately after, implanted in the cavity with the biopsy punch. The wound was sutured, and the rats were allowed to wake without any further intervention. All rats became fully conscious within 2 h after surgery and did not display any sign of distress. In control rats, the same surgical procedure was also performed, but no scaffold was implanted. Ketoprofen was administered for 2 days after surgery. Two groups of rats were set up: one group consisted of 9 rats (3 implanted with SF-HA sponges, 3 implanted with SF-HA-hep sponges, and 3 cavity controls - with no implants), and was intended for the short-term study (euthanized after 7 days) while the other group, consisted of 12 rats (4 implanted with SF-HA sponges, 4 with SF-HA-hep sponges and 4 controls), was intended for the long-term follow-up (euthanized after 118 days). MRI follow-up was performed on days 6 and 76 post-implantation.

2.3.2.2. Histology. After euthanasia, the brains were collected and subsequently fixed in formalin for a duration of 10 days, followed by paraffin embedding. Next, 5 µm thick sections were obtained using an HM340E Microm Microtech microtome (France) and stained with hematoxylin and eosin (HE) for analysis. The histopathological parameters considered included multinucleated giant cells, acute inflammatory cells, necrosis, chronic inflammatory cells, neoangiogenesis, hemorrhage, hemosiderin deposition, and mineralization. These parameters were evaluated in randomly selected fields under 40× magnification in the tissue sections. The analyses were conducted at the Department of Cellular and Tissue Pathology, centre Hospitalier Universitaire d'Angers (CHU-Angers, France). Microscopic images were captured using an Olympus microscope.

2.3.3. Evaluation of SDF-1α release in rat brains

To study the potential release of SDF-1α from the sponge to the brain, an SDF-1α coupled with Alexa Fluor 647 (AF-SDF-1α) at the C terminal (Almac, Scotland) was used. The SF-HA-Hep sponge was used for further *in vivo* experiments, as the SF-HA sponge was mostly degraded after 7 days. The same methods to prepare the sponges, including cutting and sterilization, were used as cited before. Afterward, the 3 mm diameter sponges were taken out of the biopsy punch, the PBS excess was taken out by blotting them on a gauze, producing slight dehydration, and rehydrated by

adding 3 µL of AF-SDF-1α (150 ng) on the top of the sponge to finally implant them in the cavity of Fischer rats as described in Section 2.3.2.1. With this process, the full volume of AF-SDF-1α was absorbed by the sponge, resulting in a theoretical 100 % loading. Rats were euthanized after 7 days, and the brains were snap-frozen in isopentane and stored at −80 °C right after collection. Tissues were cut coronally in the region of interest with a Cryostat Leica CM3050 S (Leica Biosystems, Nussloch, Germany) to obtain 10 µm thick slices that were deposited on gelatinated Superfrost slides (Thermo Fisher Scientific, Braunschweig, Germany), and kept at −20 °C until immunolabeling.

2.3.4. Evaluation of the sponge's performance in vivo

To assess the GB cell attractant capacity of sponges *in vivo*, two orthotopic models were tested in nude female rats, aged 8 to 10 weeks. In the first model, 5 × 10^3 U87MG-CXCR4+ cells were injected into the striatum (P: +0.8 mm; L: −3 mm (right from the bregma); D: −2.5 mm from the cortex surface). After 10 days of tumor development, a 3-mm diameter and ∼2-mm depth resection cavity was performed in the same vertical axis of cell injection using a biopsy punch. The tissue was then aspirated, and SF-HA-Hep sponges (3-mm diameter and 2-mm height) were implanted loaded or not with 100 pmol of SDF-1α. After 7 days, animals were euthanized, and brains were collected and snapfrozen at −80 °C until analysis. GB cell identification was performed by RFP, CXCR4 and Ki67 analysis by IHC-IF.

In the second model, a resection cavity was created (P: +0.8 mm; L: −2.9mm (right from the bregma); D: ∼ −2 mm from the cortex surface). SF-HA-Hep sponges (3-mm diameter and 2-mm height) were implanted loaded or not with 100 pmol of SDF-1α in 5 µL of PBS. Following this, 2.5 × 10^4 U87MG-CXCR4+ cells were injected at 1 mm posterior from the edge of the resection (Stereotactic coordinates: P: −1.7, L: −2.9, D: −2 mm from the surface of the brain). Excess blood was removed with sterile gauze, the cavities were closed with non-absorbable bone wax and the wound was sutured.

The animals recovered after 2 h and did not show signs of distress. Animals were monitored daily, observing food and water intake, also weights were recorded. After 7 days, euthanasia was conducted, and all brains were extracted, snap-frozen and kept at −80 °C until analysis. The experimental design consisted of three groups: resection control, PBS swollen sponges, and sponges loaded with SDF-1α ($n = 3$). A survival experiment was performed using the same latter surgery procedures, but 1 × 10^3 U87MG-CXCR4+ cells were injected instead ($n = 6$ per group). Animals were followed by MRI weekly and euthanized at defined endpoints.

2.3.5. MRI analysis

MRI scans were performed with a Bruker Biospec 70/20 system operating at 7T, under isoflurane (0.5 % 1 L/min O_2) anesthesia, with the monitoring of respiratory parameters. T2-weighted images were acquired with a multi-spin echo sequence [FOV = 35×35 mm, slice thickness = 0.8 mm, spacing between slices = 1.1 mm, matrix 256×256, TR = 2.5 s, TE = 33 ms].

2.3.6. Immunohistochemistry and immunofluorescence

For the SDF-1α release study, 10 µm sections were fixed with PFA 4 % (w/v) at 4 °C for 20 min, permeabilized with 0.25 % (w/v) Triton X-100 in PBS for 10 min and saturated with NGS 10 % (w/v) in PBS for 2 h. They were then incubated overnight at 4 °C with polyclonal rabbit IgG anti-SDF-1α (1:500) (Abcam, Cambridge) followed by 1 h incubation at RT with the secondary antibody goat anti-rabbit AF 488 (#4412 Cell Signaling). Cell nuclei were stained with DAPI (1:2000, Thermo Fisher Scientific, Waltham, MA) before mounting sections with Dako fluorescence mounting media (Dako, CA, USA). Stained sections were visualized using a confocal microscope Leica TCS SP8 AOBS (Leica Microsystems, Wetzlar, Germany).

For the sponge's bioperformance study, 16 µm sections were fixed for 10 min in methanol at −20 °C and rehydrated in PBS (3 washes). After saturation in PBS/4 %BSA/10 %NGS/0.25 % TritonX100 for 1 h, sections were probed with the primary antibodies as follows: anti-CXCR4 polyclonal (1:2500, #PA3–305-Invitrogen) which does not cross-react with rat tissue, or anti-Ki67 (1:200, ab16667-ABCAM), both overnight at 4 °C in a humidified chamber. After washing (3x in PBS) the slices were incubated with a biotinylated secondary Ab (anti-mouse or anti-rabbit, 1:100 in PBS/4 %BSA, Vector Laboratories) for 1 h at RT. Slices were re-washed and incubated with Streptavidin-FITC (1:500, Interchim) or Streptevidin-AF647 (1:500, Life Technologies) in PBS for 45 min at RT. After washing, slices were incubated with DAPI, and finally with Sudan Black for 15 min before mounting slides. Fluorescence was analyzed in a Leyca confocal microscope.

2.4. Statistical analysis

Data are presented as mean ± SEM. Data were statistically analyzed using an ANOVA test with Prism 7 software. Tukey's multiple comparison test was used to compare individual groups. For analysis considering only two groups, a two-tailed t-test was performed. UACMA data was analyzed with a two-tailed paired t-test. In all statistical comparisons $p < 0.05$ was considered statistically significant. For the survival analysis, all and single groups were compared using the Log-rank (Mantel-Cox).

3. Results

In vitro studies

3.1. U87MG-CXCR4+ cells are responsive to SDF-1α

Human GB U87MG cells were transduced for the expression of the CXCR4 receptor (U87MG-CXCR4+) and the receptor expression was confirmed by flow cytometry (Fig. 1A). Then, their molecular response was evaluated by incubation of cells with serum-free medium containing 40 ng/mL of SDF-1α. Results showed an increased p-Akt/Akt ratio after 15 min, which was maintained at 1 h of incubation with SDF-1α, whereas the p-Erk/Erk ratio was increased after 15 min of incubation but then reduced at 1 h. These results match early findings on patient de-novo- and recurrent-derived GB cell lines [14,21]. On the other hand, p-Paxillin/Paxillin ratio was gradually increased at 15 min and 1 h of evaluation (Fig. 1B), suggesting a gradual formation of focal adhesions [22].

To assess the functional response of U87MG-CXCR4+ cells to SDF-1α, first, their ability to migrate across an 8-µm porous membrane was evaluated in Boyden chambers. On average, a 3-fold increase in the number of migrating cells was observed after 18 h of incubation for both 40 and 120 ng/mL of SDF-1α as compared to controls (Fig. 1C). Then, the ability of U87MG-CXCR4+ cells to leave a confined spot of agarose was measured by the length of the migrating cell halo surrounding the cell-laden agarose drop (Fig. 1D). On average a 2-fold increase in the migrated distance was observed for cells treated with 40 ng/mL of SDF-1α relative to controls.

To discriminate against the effect of proliferation, the latter assay was performed in the presence of the proliferation inhibitor Aphidicolin (ADC). Although a reduced cell hallo was observed as compared to non-ADC treated cells, approximately the same ratio of 2-fold increase in the migrated length for SDF-1α treated drops was maintained relative to controls. This result suggests that the chemoattractant effect of SDF-1α was independent of cell proliferation. Moreover, U87MG cells without receptor expression

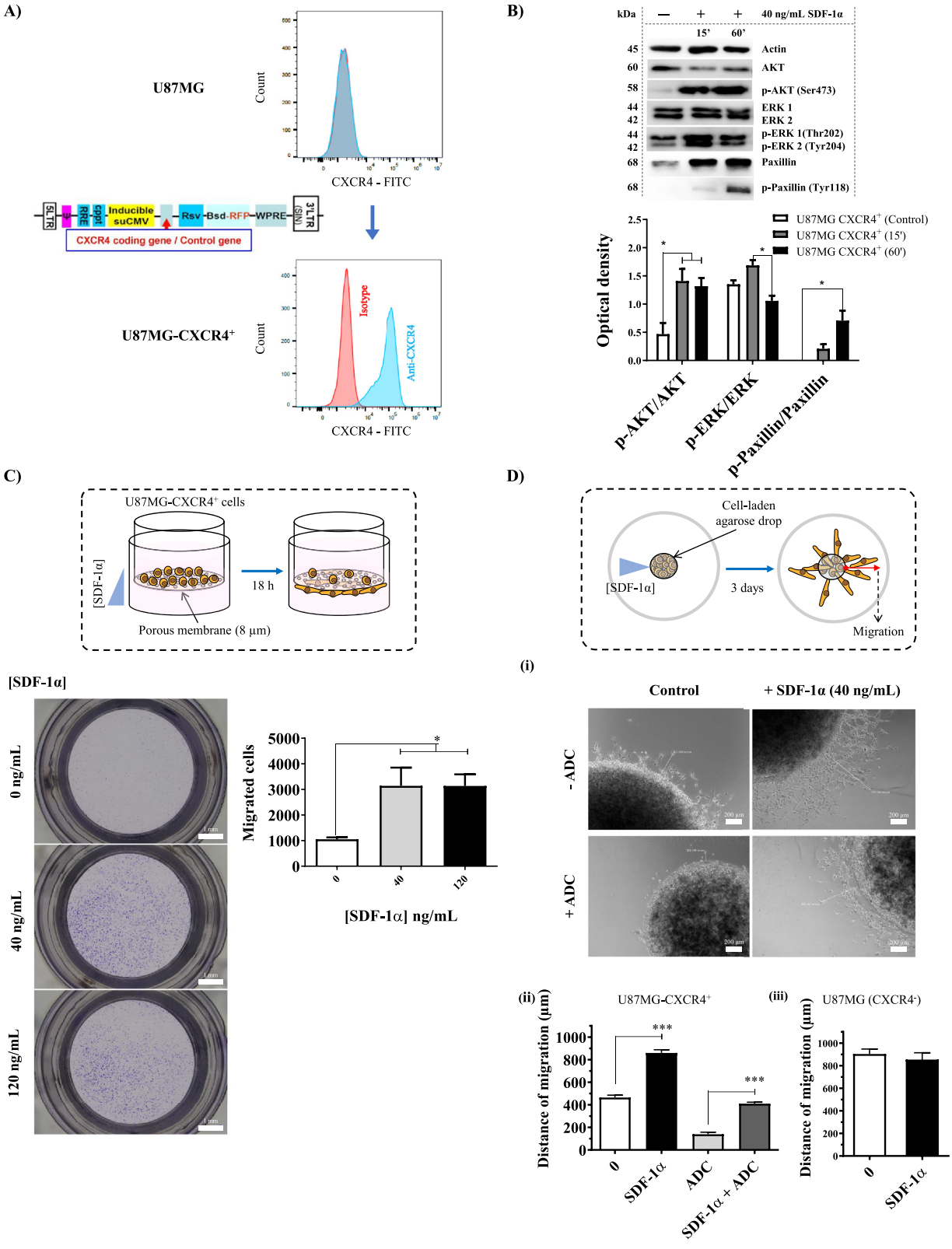

Fig. 1. Cellular model and its response to SDF-1α. A) Design of the cellular model: U87MG cells were transduced for constitutive expression of the CXCR4 receptor and red fluorescent protein (RFP). **B)** Molecular response: phosphorylation of Akt, Erk, and Paxillin shows the activation of the CXCR4/SDF-1α pathway in U87MG-CXCR4$^+$ cells in response to SDF-1α ($n = 3$). **C)** Transwell migration of U87MG-CXCR4$^+$ cells: after 18-h incubation of cells deposited on top of the porous membranes, migrating cells were more abundant in wells containing both 40 and 120 ng/mL of SDF-1α compared to controls ($n = 3$–4 replicates, with three repetitions). **D)** Agarose drop assay. (i)(ii) Migration of U87MG-CXCR4$^+$ from a confined spot of agarose was higher for cells treated with 40 ng/mL of SDF-1α as compared to controls. Inhibition of cell proliferation by the addition of Aphidicolin (+ADC) reduced the measured distance of migration but did not change the ratio of migration respective to controls. (iii) U87MG cells without expression of the CXCR4 receptor (U87MG-CXCR4$^-$) did not show a significative difference when treated with SDF-1α compared to control drops ($n = 3$ replicates, with two repetitions). Levels of significance are: $*$: $p < 0.05$, $**$: $p < 0.01$, $***$: $p < 0.001$.

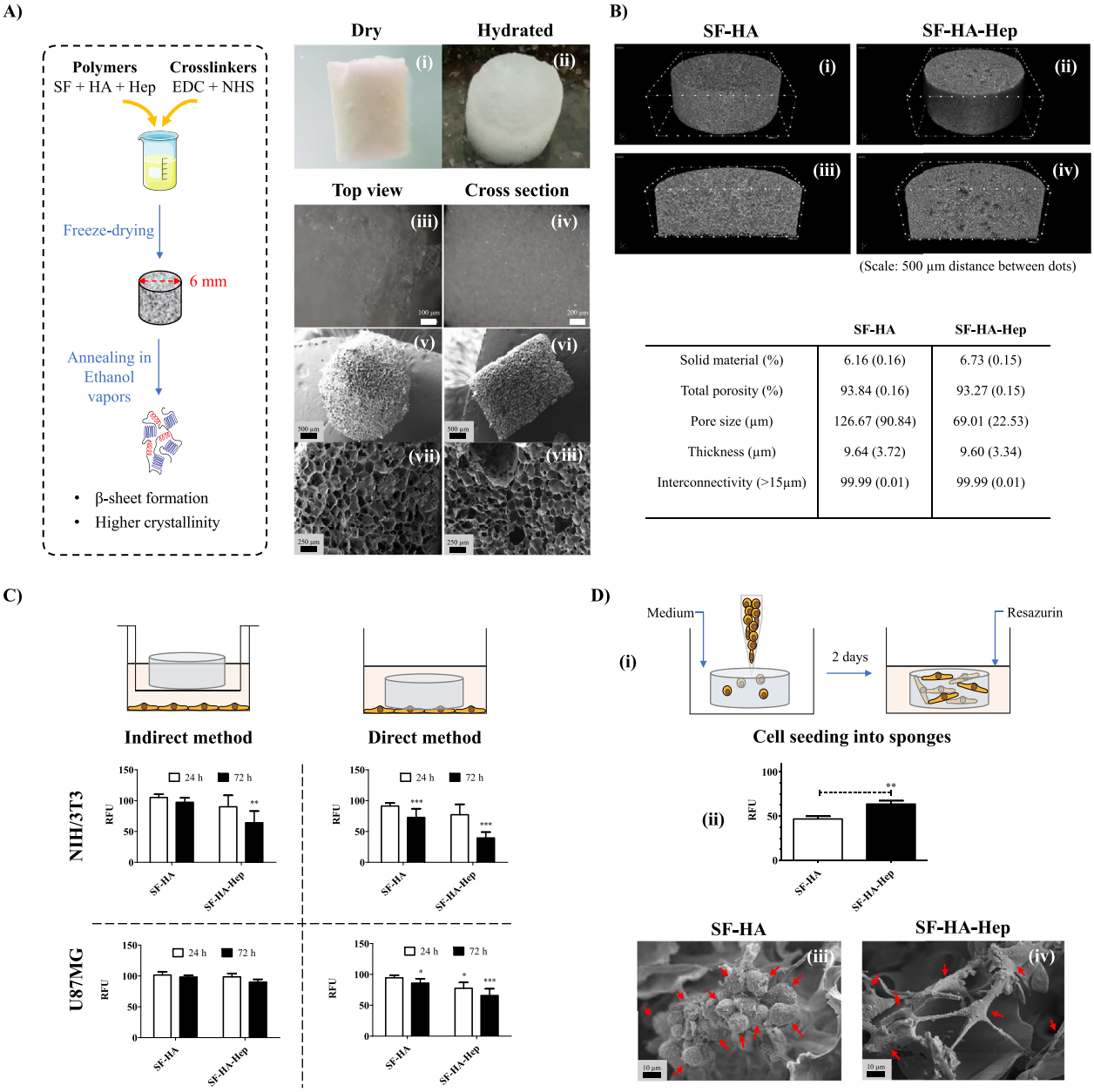

Fig. 2. Aerogel sponges, synthesis, structure, and cellular response. A) Synthesis and structure of the silk fibroin (SF), hyaluronic acid (HA), and heparin (Hep) sponges. Dry SF-HA-Hep sponges (i) rapidly absorb PBS and maintain their shape (ii). Stereomicroscopic images [(iii) and (iv)], and scanning electron micrographs [(v), (vi), (vii) and (viii)] showing the superficial and cross-sectional porous structure of SF-HA-Hep sponges. B) Microcomputed tomography (µCT) images for the evaluation of the porosity of sponges, the size and wall thickness of their pores, and the percentage of their connected pores with troughs > 15 µm. Depicted are representative µCT images of superficial [(i) and (ii)], and cross sections [(iii) and (iv)] of sponges without heparin (SF-HA) and with 1 % Heparin (SF-HA-Hep). C) The cell response of NIH/3T3 and U87MG cells after incubation with leachables from sponges (indirect method) and after direct contact of sponges with a cell monolayer (direct method) was evaluated using the resazurin assay. Depicted in the graphs are the percentages of the relative fluorescent units (RFU) respective to control wells that contained no scaffolds ($n = 3$ replicates, with three repetitions). D) The response of cells directly seeded into scaffolds. U87MG cells were directly deposited into scaffolds. After 2 days, the cellular response in SF-HA and SF-HA-Hep scaffolds was evaluated by incubation with media containing resazurin (i). The produced fluorescence in the media was normalized to control wells with cells seeded on plastic and is expressed as the percentages of RFU (ii) ($n = 5$ replicates, with 2 repetitions). U87MG cells (red arrows) seen under scanning electron microscopy 3 days after seeding in SF-HA sponges (iii) and SF-HA-Hep sponges (iv). Levels of significance are: ∗: $p < 0.05$, ∗∗: $p < 0.01$, ∗∗∗: $p < 0.001$.

(U87MG-CXCR4-) did not respond to SDF-1α, in terms of chemoattraction, as observed by the equal distances of migration for both non-treated and treated cells (Fig. 1D).

3.2. Sponges are highly porous, with interconnected pores and present shape memory

Aerogel sponges presented similar structure and physical appearance independently of heparin content (Fig. 2A). A porosity of ~ 93% was observed for both types of sponges SF-HA and SF-HA-Hep (1 % heparin). However, the pore size distribution was affected by the presence of heparin (Fig. 2B). A larger dispersion of pore sizes was observed in sponges without heparin 126.67 (90.84) µm, while sponges with heparin showed a narrower pore size distribution of on average 69.01 (22.53) µm. This reduction in the average pore size correlates to the higher content of total solids due to the addition of heparin.

The thickness of the pore walls was consistent between all types of sponges. On average, a 9.6 µm wall thickness, which represents a ~9.6/69 = ~14 % of the diameter of a pore including walls for sponges containing heparin, reflects the spongy nature of the scaffolds. Thirdly, all sponges showed open, interconnected pores. This can be observed by tracking the maximal length of the path with troughs larger than 15 µm that can be followed without interruption in both orthogonal axes of the cross sections of sponges. Finally, all the sponges presented shape memory as observed by their capacity to regain their original shape upon an external force was applied, and then released, over the sponges' hydrated form (**Video S1**).

3.3. SF-HA-Hep sponges present mild to moderate cytotoxicity in vitro

The viability of NIH/3T3 mouse fibroblasts and U87MG glioblastoma cells was evaluated via the indirect and direct contact methods at 24 and 72 h incubation with SF-HA and SF-HA-Hep sponges **(**Fig. 2C**)**. NIH/3T3 cells were chosen due their high sensitivity to chemical-induced toxicities (Xia et al., 2008). After 72 h of direct contact, SF-HA sponges significantly decreased the viability only for NIH/3T3 cells (71 ± 14 %). SF-HA-Hep sponges, however, presented mild cytotoxicity after 72 h of indirect contact (63 ± 19 % viability), and moderate cytotoxicity after 72 h of direct contact with NIH/3T3 cells (39 ± 9 % viability). Mild cytotoxicity was seen on U87MG cells after direct contact with SF-HA-Hep sponges at 24 (76 ± 9 % viability) and 72 h (64 ± 9 % viability).

Different washing techniques were tested aiming to eliminate traces of crosslinkers to improve the cytocompatibility of SF-HA-Hep1 % sponges. The first consisted in a 24-h wash in PBS under agitation, and the second in 5 × 30 s sonication cycles followed by agitation for 1 h in PBS. However, after 72-h of direct incubation of washed sponges with NIH/3T3 cells, no improvement was observed (**Fig. S1**). To determine whether EDC and NHS or Heparin were responsible for this cytotoxicity, two new sponges were produced. The first was composed of SF and HA crosslinked with the same concentration of crosslinkers as SF-HA-Hep (C_{EDC} = 15 mg/mL, C_{NHS} = 5.5 mg/mL) and was called SF-HA(+). The second was composed of SF, HA and Hep crosslinked with the same concentration of crosslinkers as SF-HA (C_{EDC} = 5 mg/mL, C_{NHS} = 1.8 mg/mL) and was called SF-HA-Hep(-). Because of the lower concentration of crosslinkers in the SF-HA-Hep(-) sponge, its shape was lost in the media.

Sponges with the same concentration of crosslinkers showed the same cytotoxicity, with a lower concentration of crosslinker leading to an increase in viability (**Fig. S1**). A tradeoff between stability and cytotoxicity had to be made, and therefore the original SF-HA-Hep1 % sponge was kept for further studies. Additional evaluation of its 24-h cytotoxicity by the direct contact method on cells resemblant to resident cells of the normal brain parenchyma was performed. In this case, murine BV-2 and human HMC3 microglial cells showed a viability of 64.4 and 82.3 %, respectively (**Fig. S2**).

3.4. The matrix of SF-HA-Hep sponges allowed a better U87MG GB cell response

To assess the response of cells in the scaffold's matrix, U87MG cells were directly deposited into the sponges as a cell suspension and cultured for 2 days. The cell response was evaluated by the resazurin assay (Fig. 2D-i). Results showed that SF-HA-Hep sponges allowed a better response compared to SF-HA sponges (Fig. 2D-ii). After 3 days of culture, SEM images showed cell aggregates in SF-HA sponges with no or little spreading of their soma (Fig. 2D-iii), whereas cells in SF-HA-Hep1 % sponges attached, spread, and formed large protrusions, suggesting a better interaction with GB cells (Fig. 2D-iv).

3.5. SDF-1α-loaded sponges directionally attract U87MG-CXCR4+ cells in vitro

To evaluate the chemoattractant capacity *in vitro*, sponges loaded with SDF-1α (10 and/or 100 pmol) were added in the right well, contiguous to a well containing U87MG-CXCR4+ cells in an agarose gel (Fig. 3). A well containing only PBS was also included to the left. After 3 days of culture with the addition of Aphidicolin as a proliferation inhibitor, results showed that there was a larger area of cells that migrated under the agarose towards the SDF-1α-loaded sponges as compared to controls located in the wells left to the cells. The migrated area depended on the dose of SDF-1α and the percentage of FBS used for cell seeding. Indeed, FBS was necessary for cells to adhere. This effect corresponded to a 3-fold increase of the invaded area for the 10 pmol loading and an 11.3-fold increase for the 100 pmol loading as compared to controls, in the case of 1 % FBS seeded cells (Fig. 3A-iii). A larger area in both directions, towards the sponges and controls, was observed when cells were seeded with medium containing 10 % FBS. However, increasing area ratios of 2.2-fold and 3-fold showed preferential migration of cells towards the sponges loaded with 10 and 100 pmol of SDF-1α, respectively (Fig. 3A-iii). To evaluate if the sponges alone were able to attract GB cells *in vitro*, the experiment was repeated with sponges containing only PBS compared to wells filled with only PBS (Fig. 3B-i). Results showed no significant difference in the areas of cell migration. When SDF-1α-loaded sponges were compared to sponges containing only PBS, only the former were able to show cell attraction (Fig. 3B-iii), showing a similar pattern than agarose gels where only PBS was used as a negative control (Fig. 3B-ii**).**

3.6. SDF-1α in SF-HA-Hep sponges enhanced their colonization in vitro

To assess the cell hosting capacity of sponges, single ~ 200-µm U87MG-CXCR4+ spheroids were cultured on top of SF-HA-Hep sponges that were loaded or not with 100 pmol of SDF-1α (Fig. 4B). Results showed that after 6 days of culture, there was a 1.4-fold larger area of glioma spheroids attachment on the surface of the sponges loaded with SDF-1α in relation to control sponges loaded with PBS (Fig. 4B-iii). In addition, a 1.6-fold larger infiltrated area and a 1.3-fold maximal infiltrated length in the sponges loaded with SDF-1α were observed compared to controls. However, cells remained within the contours of the glioma spheroids and did not spread out ubiquitously within the sponge in the 6-day time frame of the experiment.

***In vivo* studies**

3.7. Sponges are biocompatible and biodegradable in vivo

SF-HA and SF-HA-Hep sponges were implanted in the resection cavities of Fisher rats to evaluate the foreign body reaction in the brain as well as their biodegradability (Fig. 5). MRI images showed the presence of the sponges at D6 from implantation but completely degraded after 76 days as shown by the watery content in the cavities (Fig. 5A). SF-HA sponges were mostly absorbed after one week of implantation, which was confirmed by histological analysis (Fig. 5B). The cellular response was characteristic of a foreign body reaction with an acute inflammatory response at week one post-implantation, with the presence of polymorphonuclear (PMN) cells that was more important for SF-HA-Hep sponges compared to SF-HA sponges.

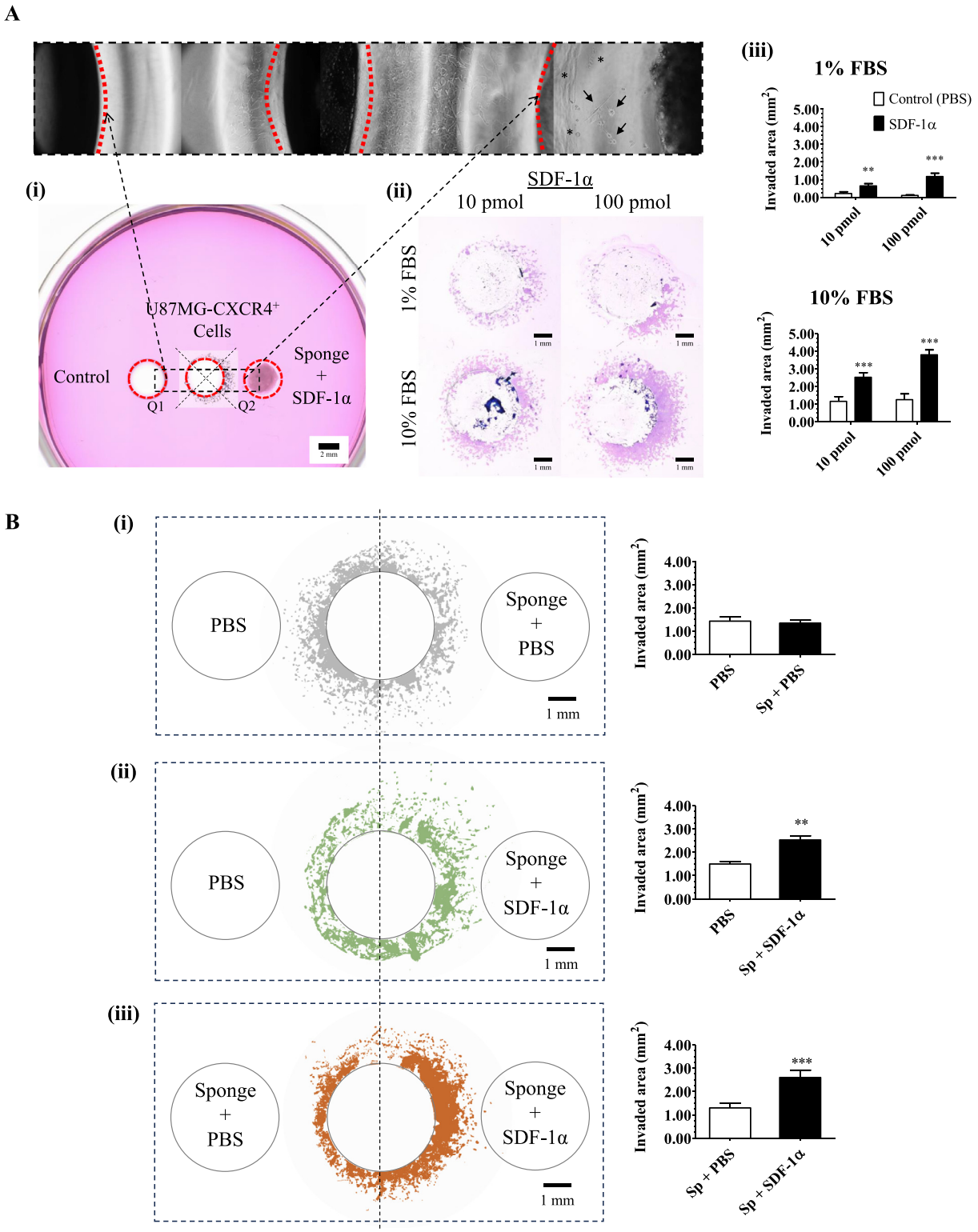

Fig. 3. *In vitro* cellular attraction. A) *In vitro* chemoattractant capacity of SDF-1α-loaded sponges: (i) agarose gel showing the disposition of cells (center well), sponges (right well), and control wells containing PBS (left well) to assess the induction of directional migration. Top panel: images (10x objective) of a representative experiment on day three after cell seeding. The assembled image shows the pattern of cell migration under the agarose gel. Some cells were detected near the sponges loaded with SDF-1α (100 pmol) (black arrows), with some cells undergoing cell death (asterisks). Of note is the "squeezed" shape of cells under the agarose, whereas cells that invade the right agarose-gel-free well regain a "spindle-like" morphology. (ii) Giemsa staining of cells that migrated under the agarose after three days of incubation. Cells were seeded in media containing either 1 % or 10 % FBS and 5 μg/mL of Aphidicolin as a proliferation inhibitor. (iii) Quantification of the cell area of the binary images in the most proximal quarters (Q) to either control wells (Q1) or sponges (Q2) as depicted in the representative image in the center well of (i) ($n = 3$ replicates, with three repetitions). B) The effect of the sponges alone containing only PBS (i) or of sponges loaded with 100 pmol of SDF-1α (ii), as compared to wells loaded with only PBS (left wells). (iii) The effect of sponges containing 100 pmol of SDF-1α vs. sponges loaded with only PBS. ($n = 3$ replicates, with three repetitions). Levels of significance are: ∗: $p < 0.05$, ∗∗: $p < 0.01$, ∗∗∗: $p < 0.001$.

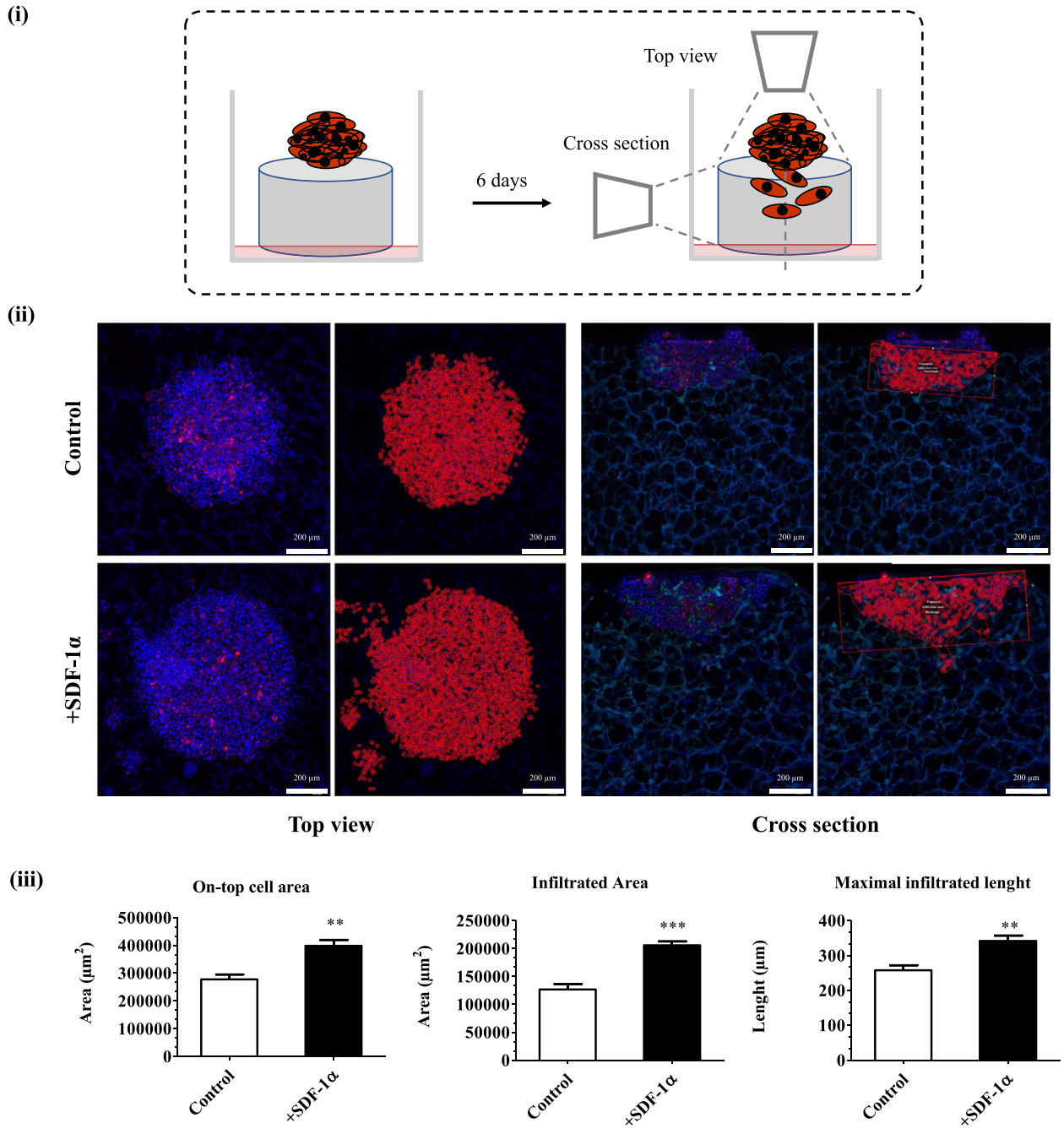

Fig. 4. *In vitro* cellular colonization of sponges. (i) Representation of the spheroid culture assay for the evaluation of the capacity of SF-HA-Hep sponges to be colonized by GB cells coming from GB spheroids. A single U87MG-CXCR4^{+} gliomaspheroid was deposited on top of a SF-HA-Hep sponge loaded or not with SDF-1α. After 6 days of culture, the on-top cell area, the infiltrated cross-sectional area, and the maximal infiltrated length were imaged (ii) and quantified (iii) ($n = 3$; 2 experimental repetitions). Levels of significance are: $*$: $p < 0.05$, $**$: $p < 0.01$, $***$: $p < 0.001$.

The presence of multinucleated giant cells was rare, but the concomitant presence of macrophages and lymphocytes showing up from the initial stages after implantation demonstrates a process of debridement and chronic inflammation that was prolonged to up to the third month post-implantation. The formation of new blood vessels was more evident on day 7 of evaluation for all groups suggesting that the brain damage caused by the surgical resection and the consequent signals induced this neoangiogenic response. On the third month of evaluation, the acute inflammation was resolved, and the chronic inflammation lessened. Interestingly, only the cavities of rats implanted with sponges kept some lymphocytes in the long term compared to cavity controls alone. The presence of hemosiderin-laden macrophages and calcification zones (mineralization) showed the late stages of cicatrization. Overall, the residual cavities were porencephalic, i.e., filled with resident cerebral cells but with the loss of brain matter, however no collagen deposition nor fibrotic tissue was observed in the implantation zone, suggesting a good reabsorption of the sponges without the formation of a scar. As SF-HA sponges were mostly degraded within the first week of implantation, SF-HA-Hep sponges were chosen for further experiments.

A)

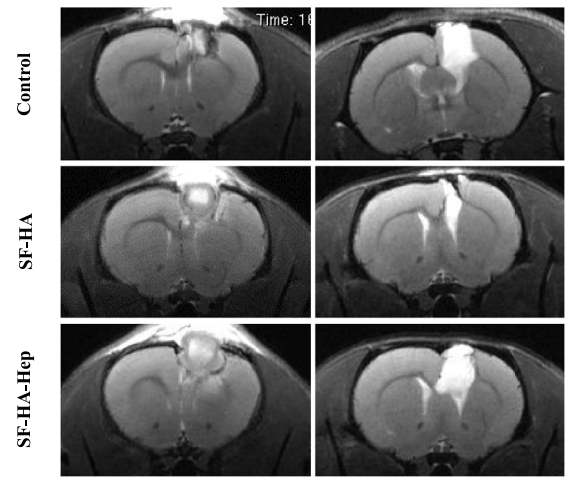

B)

Day 7			Day 118			[- -/+ + ++ +++]
Cavity Control	SF-HA	SF-HA-Hep	Cavity Control	SF-HA	SF-HA-Hep	
-	-	-/+	-	-	-	Multinucleated Giant cells
+	-	++	-	-	-	Acute inflammatory cells (PMN cells)
-	-	++	-	-	-	Necrosis
++	++	+	-	+	+	Chronic inflammatory cells
++	+	+	-	-	-	Neoangiogenesis
-	-	-	-	-	-	Haemorrhage
-/+	-	-	+	++	+	Hemosiderin
+	+	-	-/+	+	+	Mineralization

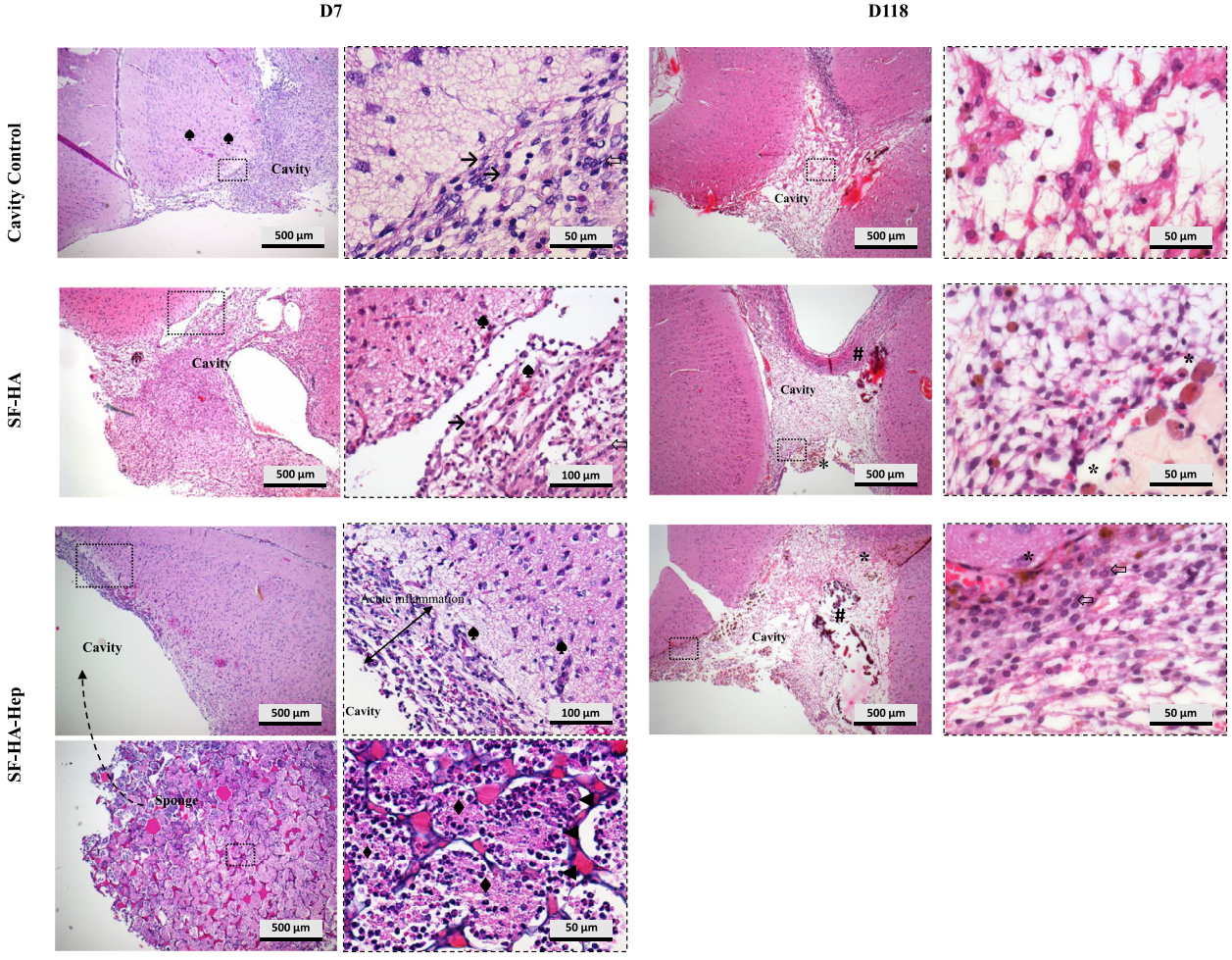

Fig. 5. *In vivo* biocompatibility and biodegradability of sponges. A) MRI scans of brains with implanted sponges. B) Characterization of the *in vivo* cellular response to implanted sponges in the rat brain cortex. Histological (H&E) staining (nuclei: blue/purple; cytoplasm: pink). SF-HA sponges were completely degraded after 7 days, while SF-HA-Hep sponges were still present. A representative image is shown of a SF-HA-Hep sponge that came out of the cavity during the slicing process (bottom left panel). Left panels: H&E representative images 7 days post-implantation showed an acute inflammatory response in rats implanted with SF-HA-Hep sponges. The acute response was less marked in the other groups. There was a local chronic inflammatory response with the presence of lymphocytes that were more frequent in the cavity controls and in SF-HA implanted rats. At this 1-week time point, the formation of blood vessels (neoangiogenesis) was observed in all groups. Right panels: After 3 months, the acute inflammation was resolved, and the chronic inflammation lessened in the control cavity and SF-HA groups and remained in the SF-HA-Hep group. At this 3-month time point, mineralization and hemosiderin deposition were observed in all groups. Symbols are as follows: infiltrating polymorphonuclear (PMN) cells (◂), Necrosis (♦), macrophages (→), lymphocytes (⇦), neoangiogenesis (♠), hemosiderin (*), mineralization (#). Scores are as follows: (−) = nil, (-/+) = rare, (+) = mild, (++) = moderate, and (+++) = marked. Interrupted-line bordered images are magnifications of the smaller squares indicated in their respective left images.

3.8. SDF-1α was retained in SF-HA-Hep sponges in vivo

To evaluate the *in vivo* biodistribution of SDF-1α in the brain after the sponge's implantation, SF-HA-Hep sponges were loaded with 150 ng of AF-647 tagged SDF-1α and implanted in the resection cavities of Fisher rats. Results showed that 7 days post-implantation, AF647-SDF-1α was detected inside the sponges, and in the margins of the resection cavity as bulges detaching from the edges of the sponges that were undergoing degradation; but was not detected in the brain tissues beyond the resection limits (Fig. 6A). Interestingly, AF647-SDF-1α was distributed as droplets of about 10–100 μm diameter which corresponded to the internal structures observed in the sponges (Fig. 6A-third panel). Endogenous SDF-1α was stained indirectly with an antibody coupled with FITC and was distinguished from the exogenous SDF-1α that was loaded into the sponges, as the latter was not recognized by the primary antibody (Fig. 6B). Endogenous SDF-1α was found only scarcely expressed in small blood vessels surrounding the resection cavity. Interestingly, more nuclei were observed inside the sponges containing SDF-1α compared to the brain tissue. This correlates with the colonization of sponges by PMN cells as observed in Fig.5B.

3.9. CXCR4+ GB cells interacted with SDF-1α loaded sponges 7 days post-implantation

To assess the GB cell attractant capacity of sponges *in vivo*, two orthotopic models were tested in nude rats. In the first model, 5×10^3 U87MG-CXCR4+ cells were injected into the striatum. After 10 days of tumor development, a ~2-mm depth resection cavity was performed in the same vertical axis of cell injection, and SF-HA-Hep sponges were implanted loaded or not with SDF-1α. After 7 days, animals were euthanized, and brains were collected and analyzed by IHC-IF. Cell tracking by RFP, CXCR4 and Ki67 expression revealed colonization in only one implant loaded with SDF-1α (out of 3 animals) (**Fig. S3**). Although this experiment showed that SDF-1α-loaded sponges can be colonized by tumor cells after resection, the main complication found here was the lack of a reproducible resection. For instance, the tumor was completely removed in some cases and the distances between the tumors and scaffolds were not reproducible. To overcome this limitation, the second experimental set-up consisted in placing the implants and cells distanced from ~1 mm in the horizontal plane of the frontal brain cortex at the same time. First, SF-HA-Hep sponges with PBS or SDF-1α were implanted in the frontal cortex, followed by stereotactic injection of 2.5×10^4 U87MG-CXCR4+ cells 1 mm backward from the cavity edges (Fig. 7). Control rats were subjected to the same surgical and tumor cell injection procedures in the absence of sponges. After euthanasia, 7 days post-implantation, the brains were removed, snap-frozen and analyzed by IHC-IF. We observed a modification in the behavior of cells near the sponges compared to the cavity control alone. Cells constituting the anterior front of the tumor were able to interact with the surface of the sponges with a significant portion of CXCR4+ cells detaching from the main tumor mass towards the cavity containing the SDF-1α-loaded sponges or PBS-loaded sponges as compared to and cavity controls (Fig. 7). However, at this point, the interaction of cells with sponges was only observed at the intermediate zone between the tumor leading edge and the edge of the sponges facing it.

3.10. SF-HA-Hep sponges shaped the tumors and allowed their localized development

To assess the effect of sponges in the long term, the same orthotopic model used to evaluate the colonization of sponges was implemented, but this time 1×10^3 U87MG-CXCR4+ cells were injected. Animals were followed up until the defined endpoint, and tumor evolution was followed by MRI every week. All animals recovered within 2 h after the procedure and did not show any signs of distress. Animals behaved normally and started to present symptoms from week 4 after surgery. Results showed that the survival of rats did not improve by sponge implantation in either case loaded or not with SDF-1α (Fig. 8A) compared to cavity controls. We observed that SDF-1α tended to reduce the median of survival to 27.5 days as compared to controls (31 days), though non-significant statistically (the fact that there is one animal from the SDF-1α group crossing the other survival curves makes this non-significant). This effect correlates with the average size of the tumor that tends to be larger (as a tendency as no statistical difference was observed) for rats implanted with SDF-1α-loaded sponges as shown in Fig. 8A **right panel**. Therefore, SDF-1α contained within the sponges may be exerting an effect on tumor evolution favoring its development. This result can be explained by the fact that no killing signal was included in the study. However, we observed an effect of the sponges on the tumor shape and localization. Interestingly, the shape of the tumors fitted better to the projections' shape of the cross sections of the sponges in the three axes imaged and they were more rounded compared to the tumors where sponges were not present (Fig. 8B). Indeed, the reduced tumoral areas outside the projection of sponges, suggest that the tumor is better confined in the volume behold by the sponge's structure. This result highlights the relevance of the sponge implantation as a strategy to confine the tumor in a controllable area and confer a spherical shape that can facilitate their further treatment.

4. Discussion

The main problem facing glioblastoma therapy is the infiltrative nature of GB cells remaining after standard treatment. cDNA expression analysis revealed that CXCR4 is overexpressed in 57 % of primary glioblastoma (GB) tumors and in 88 % of GB cell lines that were analyzed [23]. CXCR4 expression is considered a prognostic marker in gliomas. Patients with CXCR4-positive GB had a reduced postoperative life expectancy [24]. CXCR4 was expressed in more than 50 % of astrocytomas and 100 % activated form (phosphorylated) in grades 2–4 astrocytomas and 76 % in grade 1 astrocytomas [25]. Previously, it was shown that the CXCR4 receptor confers to GB cells increased infiltrative capacity into the brain parenchyma [18], and that the CXCR4/SDF-1α axis is related to the chemotaxis attraction of GB cells *in vitro* [14,26] and of glioma stem cells (GSCs) to the tumor vasculature [27]. Here, a rupture concept was investigated. The strategy was to exploit the CXCR4/SDF-1α axis to attract GB cells to a confining biodeposit consisting of a SF-HA-Hep sponge. This study aimed to investigate the preclinical feasibility and benefit of a new interventional approach using SDF-1α-loaded SF-HA-Hep aerogel sponges as implantable scaffolds into the brain resection cavity. Fischer rats were used to assess the *in vivo* biocompatibility of scaffolds to observe the complete foreign body reaction. However, to evaluate the *in vivo* performance of sponges, athymic nude rats were chosen because of the human cellular model that was used. The sponges are biodegradable. They were well tolerated for more than 3 months and reabsorbed after implantation into rat brains. The disappearance of the sponges is attributed to the inherent biodegradability of the scaffolds, primarily through hydrolysis and solubilization of the components. *In vitro* studies reported 85 % degradation within 3 weeks [17], under conditions mimicking *in vivo* enzyme presence. This gradual degradation can facilitate temporary accommodation of cancer cells within the cavity, minimizing the risk of long-term adverse reactions or the need for surgical removal. Their shape memory permitted fitting into the resection

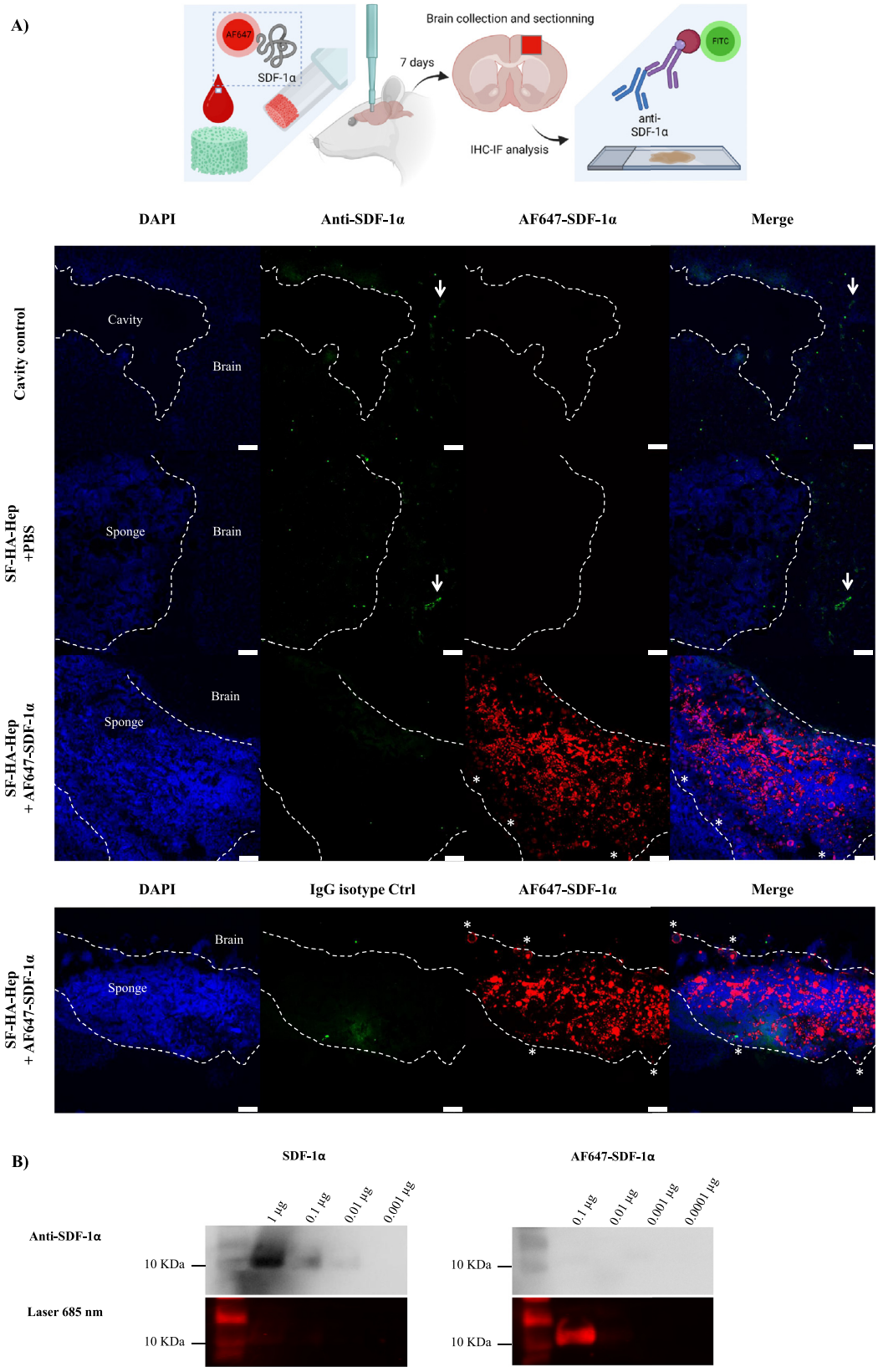

Fig. 6. *In vivo* distribution of SDF-1α. A) Implantation of SF-HA-Hep sponges containing SDF-1α tagged with AF-647, in the resection cavity in the frontal cortex of Fisher rats (Created with BioRender.com). Control sponges contained only PBS. Seven days after implantation, brains were collected and sliced. AF-647-SDF-1α was localized within the structure of the sponge (red channel, third column). Degradation of sponges was observed at their edges in contact with the borders of the resection cavity, and the detaching bulges containing AF-647-SDF-1α were located adjacent to the brain parenchyma (white asterisks). Further labeling with an anti-SDF-1α antibody and revelation by the Strep-FITC amplification method did not show the presence of AF-647-SDF-1α as the latter was not recognized by the anti-SDF-1α, see (B). The presence of small blood vessels positive for the anti-SDF-1α antibody was rarely observed in the margins of the resection (white arrows, second column, green channel). Scale bar = 100 µm. B) WB analysis for the immuno-detection of SDF-1α and AF-647-SDF-1α. The same anti-SDF-1α antibody recognized only the non-tagged SDF-1α but not the AF-647 tagged SDF-1α, which is however revealed by excitation with an IR laser.

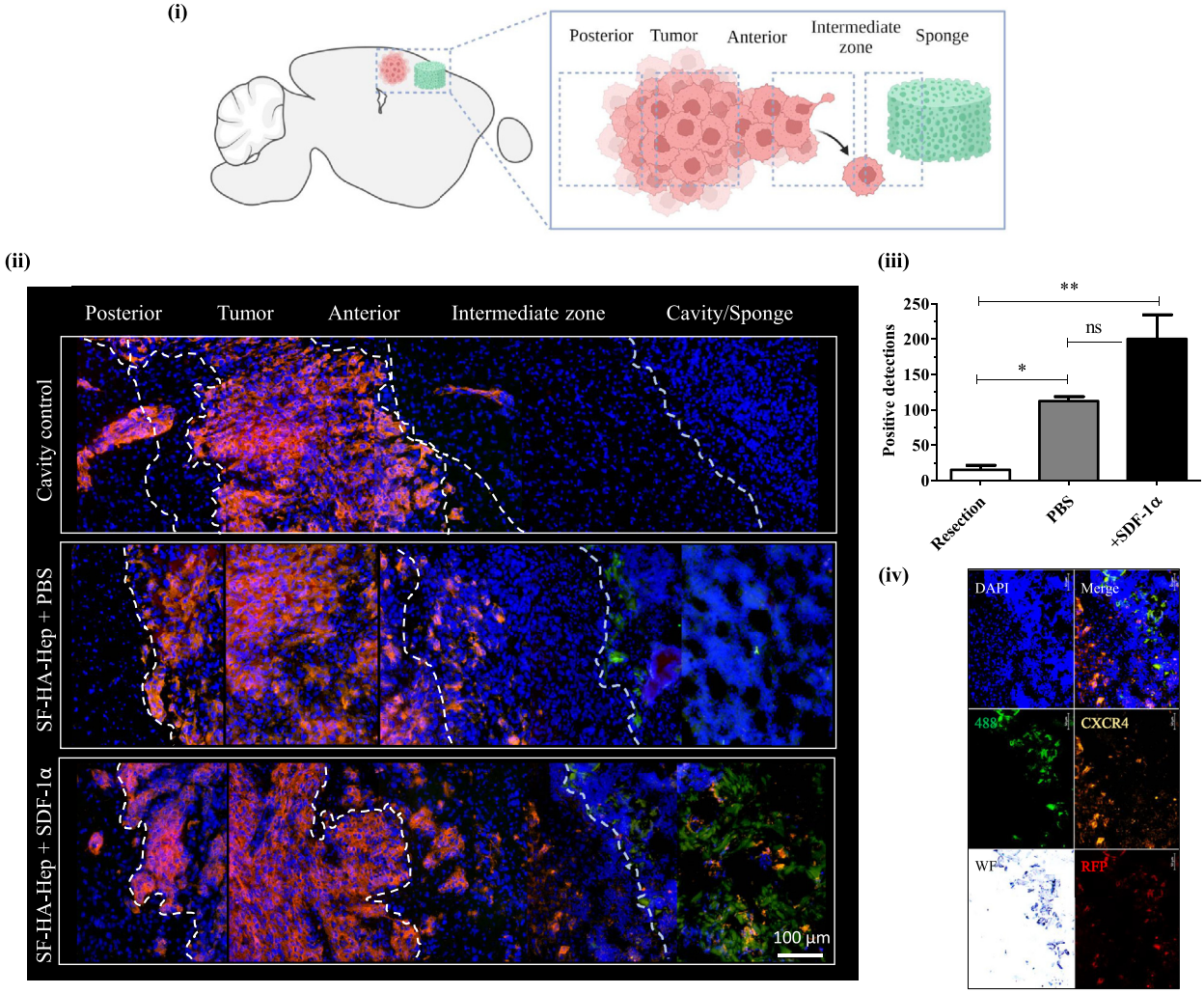

Fig. 7. *In vivo* response of GB cells to implantation of sponges. A model of the resection cavity in the brain cortex was developed in nude rats. U87MG-CXCR4^{+} cells were injected near the sponges loaded or not with SDF-1α, or near the created cavity alone (i) (Created with BioRender.com). After seven days following implantation, cell detection was performed in cryosections by RFP expression and CXCR4 immunolabeling (yellow) (ii). Depicted are the composite images resulting from the merging of the different channels. An increased cell number of dissociated cells lying in the anterior/intermediate zone between the tumor and the sponges in rats bearing SF-HA-Hep sponges loaded with SDF-1α (SF-HA-Hep + SDF-1α) or sponges alone (SF-HA-Hep + PBS) was observed as compared to rats with the resection cavity alone with no implanted sponge (iii) ($n = 3$; $*$: $p < 0.05$, $**$: $p < 0.01$). The right panel shows an example of images from single channels as follows: WF (white field), RFP (red fluorescent protein), CXCR4 (yellow), DAPI (cell nuclei), 488 (green autofluorescence of sponges) (iv).

cavities and their highly interconnected pores supported cell infiltration and growth.

To assess the *in vivo* sponges' bioperformence, a cavity resection model was developed. Due to the difficulty of reproducibility of resected tumors by using a punch biopsy pen and an aspiration method, the developed rat model here shows that concomitant placement of implants and GB cells is feasible to investigate the functionality of interventional scaffolds in a model of the residual disease were infiltrating cells are situated adjacent to the cavities in the brain parenchyma. This strategy might be used to assess different scenarios including the distance between cells and scaffolds, and the number of injected cells. Here, by 1-mm distant placement of GB cells relative to resected zones, it was revealed that GB cells interacted with the sponges 7 days post-implantation. Serving as a chemokine reservoir in the tissue, SDF-1α remained within the sponges after 7 days of implantation.

In vitro, sponges loaded with SDF-1α directionally attracted U87MG-CXCR4+ GB cells and enhanced cell colonization within the scaffold. The function of SDF-1α is observed in the under-agarose assay *in vitro* from a distance that is 2-fold larger than the sponge implanted *in vivo*. The sponges alone did not show a difference relative to only wells containing PBS (Fig. 3B-i). And sponges loaded with SDF-1α attracted cells vs sponges alone (Fig. 3B-iii). This means that the signaling provided by the released SDF-1α is necessary to attract GB cells distantly placed in a semi-confined site. In this case, the agarose gel provides a layer between the plastic and the gel that cells can invade. Moreover, the *in vitro* assay using tumor cells grown as spheroids demonstrated the importance of SDF-1α for improving the sponge colonization. *In vivo*, cells were injected approximately 1 mm away from sponges. This nearer placement of sponges as compared to the *in vitro* experiment, can influence the interaction of cells growing from the main tumor as observed in the intermediate zones and edges of the sponges facing the tumors in Fig. 7. Interestingly, SF-HA-Hep sponges were able to shape and locate the tumors inside the cavities. The effect of shaping of the tumor by sponges alone (Fig. 8D) can be explained by the attraction of cells by mechanisms yet undetermined and independent from SDF-1α. *In vivo*, on day 7 after cell injection, there was no significant difference between the positive detections of cells in the intermediate zone located be-

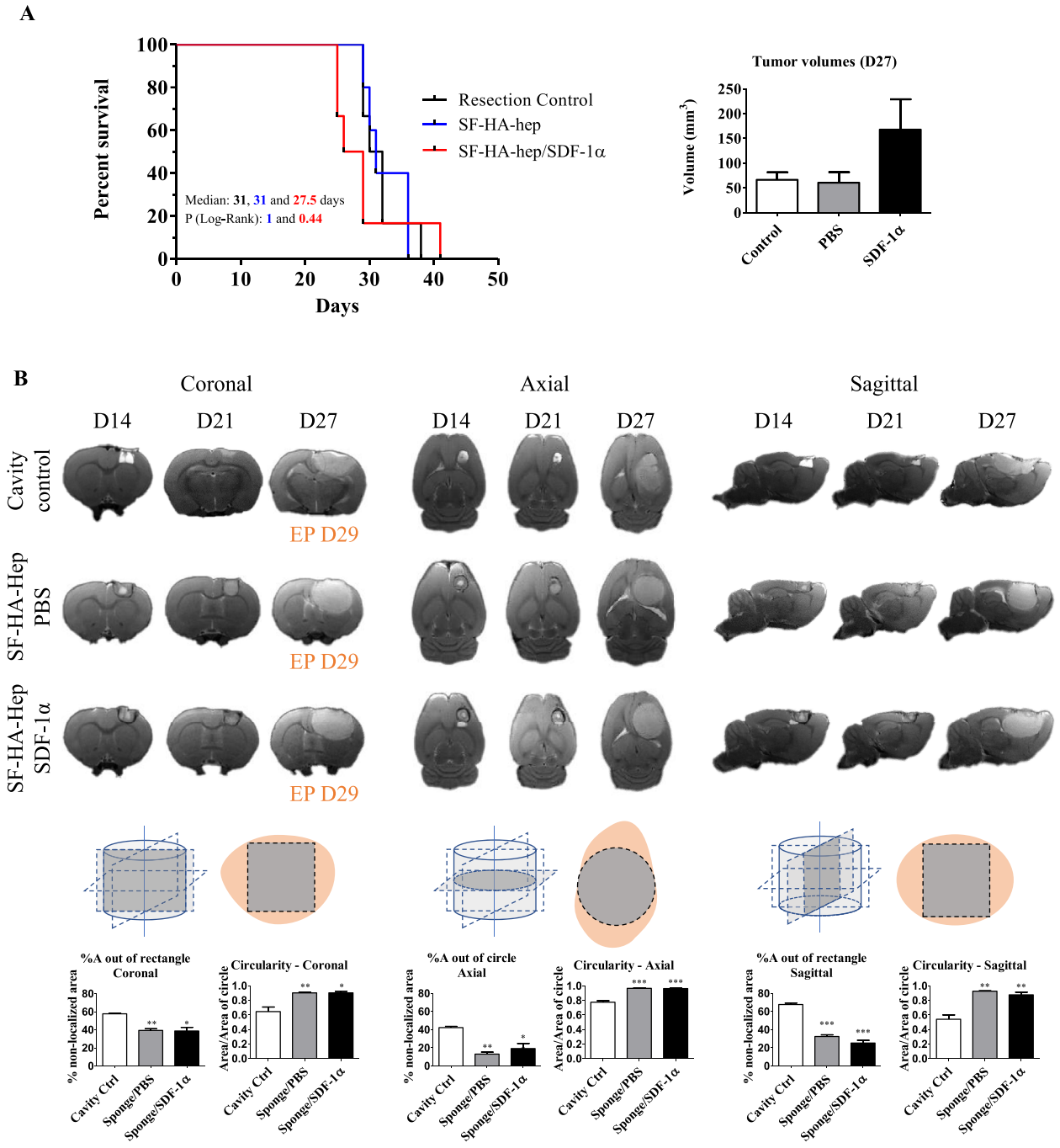

Fig. 8. Evolution of tumor growth and survival analysis of implanted rats vs cavity controls. A) Survival Analysis. Although no significant statistical difference is observed between groups, the calculated smaller median survival (27.5 d) for sponges loaded with SDF-1α correlates with a higher average tumor volume on day 27 (as a tendency as no statistical difference is observed, $P = 0.059$). **B)** The shape of the tumor is affected by the presence or absence of sponges. The area of the tumor out of the enclosed and shaped cross-sectional area projected from the sponge is depicted in the lower panels. The circularity is calculated as the area of the tumor cross-section divided by the area of the adjusted circle according to the tumor perimeter ($4\pi A/P^2$). Three slices were analyzed for each projection plane for each animal ($n = 3$ animals per group). Levels of significance are: $*$: $p < 0.05$, $**$: $p < 0.01$, $***$: $p < 0.001$.

tween the tumor and sponges loaded with SDF-1α or sponges alone (Fig. 7). This can be linked to the effect of sponges loaded or not with SDF-1α on tumor shaping. The MRI images provided on Fig. 8B corresponding to day 27 suggest a displacement of the tumor towards the cavities that contained sponges. Results did not reflect a survival improvement, but this was in part expected as no killing signal was introduced. The tumor-shaping and -sitting effect occurred regardless of SDF-1α loading, suggesting it is associated with the properties of the SF-HA-Hep sponges.

4.1. SF-HA-Hep sponges as a tool for intervention: instructing the tumor ecosystem

The dynamic crosstalk between cancer cells and their environment might be interfered to instruct the GB ecosystem and potentially improve treatment. Cancer cell behavior and fate are strongly associated with non-cellular components, such as the ECM. Thus, the unique composition and architecture of the brain ECM can offer opportunities, being implemented as a target and as an instru-

ment for various therapeutic strategies [28–30]. GB cell morphology, migration and proliferation can be influenced by the composition of the biomaterial [31–33]. And parameters such as porosity, permeability and the stiffness of the scaffold can be crucial in terms of cell ingrowth, cell growth, migration, and scaffold colonization [34].

Previously, the physicochemical and mechanical similarities between the brain ECM and SF-HA-Hep sponges were described [17]. Here, we demonstrated that the multiple interconnected 69µm-pore-channel networks of SF-HA-Hep sponges played a significant role in GB cells' infiltration and spreading by providing adequate internal space and support for cell growth. Pore size is a fundamental factor implicated in the invasion and migration of GB cells [35], which occur after matrix degradation when the cross-sectional area of the interfibrillar pore is less than 7 μm^2 [36]. Above this value, cells can undergo physical deformations to squeeze through the pores of the brain ECM and migrate [37]. The spatial arrangement of the matrix fibers near primary tumor sites can influence the motility of tumor cells, and aligned fibers offer tracks that are more conducive to migration [38,39]. With this regard, Jain et al. (2014) demonstrated that aligned fibers can be used as guidance elements to direct brain resident GB cells toward an extracortical zone. In contrast, SF-HA-Hep sponges presented here did not feature any structural alignment [7]. Other works using non-aligned porous scaffolds made use of an attracting signaling strategy, trying to imitate metastatic niches. For example, De la Fuente et al. (2015) used extracellular vesicles to demonstrate the luring capacity of ovarian cancer cells when loaded into the scaffold's matrix [6]. Moreover, Azarin et al. (2015) showed that the implantation of PLG microporous scaffolds in mice mammary fat pads induced the recruitment of immune cells by cytokines including CCL22, that in turn induced the recruitment of metastatic breast cancer cells [40]. In the context of glioblastoma, Gliadel wafers used for carmustine delivery are FDA approved, but no other porous scaffolds like sponges have been used for the trapping of GB cells. This paper hence describes a new system. Porous SF-HA-Hep sponges offer the possibility of covering a larger space and taking advantage of the resection cavity after implantation. These sponges are biodegradable, so a second surgery to remove the device would not be necessary.

In the present work, we explored the effect of loading a chemoattractant into SF-HA-Hep sponges and found that SDF-1α -loaded sponges were able to attract GB cells *in vitro*. *In vivo*, clusters of tumor cells and individual cells were observed infiltrating the intermediate zone between the anterior tumor border and the sponges, which was promoted by the SDF-1α load compared to the cavity controls. However, we also found that tumor shaping and localization were favored to fit the resection cavities containing implants, and this occurred independently of SDF-1α loading. Interestingly, the shape of the tumors matched the shape of the cross-sectional projections of the sponges in the three MRI axes imaged, being more rounded when compared to the tumors where sponges were absent. This suggests that the implants exerted an attraction force from the site of cell injection toward the resection cavity. Indeed, the sponge structure was not seen anymore during the 4th week of MRI imaging. This can be explained by 1) the total colonization of the sponges by U87MG-CXCR4+ cells during the experiment, hindering the sponges' structure, 2) the complete sponge's degradation favored by the tumoral environment, and 3) the ejection of sponges by the tumor's center of mass displacement and further elimination of the sponges.

Despite not knowing the precise mechanism, the attraction of GB cells seen at the sponge-parenchyma intermediate zone after 7 days of implantation, even in the absence of SDF-1α, suggests that sponges alone may modulate GB cell behavior. Cancer cells can be guided towards laminin and hyaluronan molecules in the ECM by internal integrins and CD44 receptors respectively, and via haptotaxis by chemokines and growth factors immobilized along tracks [41,42]. In line with this, HA may have contributed to tumor cell presence inside SF-HA-Hep sponges, via CD44/HA axis [43], as the majority of U87MG-CXCR4+ cells expressed the CD44 receptor (**Fig. S4**). In addition, *in vitro* U87MG cells responded better when directly seeded into SF-HA-Hep sponges as compared to SF-HA sponges (Fig. 2D), highlighting the effect of the matrix structure and composition. Heparin and other glycosaminoglycans (GAGs) can regulate glioma cell adhesion to ECM proteins leading to cell proliferation or cell migration, according to the ECM composition, thus modulating tumor cell properties [44]. Heparin can be safely used when it is modified or covalently incorporated into scaffolds for biomedical applications [45–47] offering cell contact sites by the recruitment of molecules promoting cell adhesion. Therefore, the enhanced *in-vitro* cell response observed here could be explained by the trapping of factors from the media containing FBS such as fibronectin and vitronectin, both of which harbor heparin binding sites [48,49].

Furthermore, the strong heparin-chemokine complex was responsible for SDF-1α retention in SF-HA-Hep sponges [17,50]. As this chemokine can be rapidly turned over [51] and inactivated by nitration *in vivo* [52], the SDF-1α immobilization in the sponges combined with their slow degradation rate can offer an advantage as a reservoir reinforcing its role in haptotaxis versus chemotaxis, here pivotal for directional cell migration and colonization of the sponge. SDF-1α linked to heparin-binding domains had similar activity to the free chemokine [53]. Here, fragments of SF-HA-Hep sponges as AF647-SDF-1α bulges were seen in the edges of the brain cavities containing a high number of cell nuclei. These bulges might have induced a haptotaxis response [54].

The recruitment of immune cells in the site of scaffold implantation has been described as having a role in the creation of premetastatic niches for the capture of breast cancer cells. Leukocytes can be recruited into scaffolds reorganizing as a site of premetastasis in a murine breast cancer model. This is due in part to the secretion of soluble factors from recruited Gr1hiCD11b+ cells that can attract cancer cells [40,55]. SDF-1α is a cytokine that can be secreted by immune cells including neutrophils [56]. Despite PMN cells were recruited into the sponges, endogenous SDF-1α in the site of implantation was not detected in both implanted and mock surgery resected rats. Besides, other soluble factors can attract cancer cells which do not exclude the possible effect of implantation of SF-HA-Hep sponges alone as a premetastatic niche. Further experiments need to consider the distant placement of sponges ($>$ 1 mm) from the primary tumor site to assess their premetastatic potential.

Alternatively, the attraction driving force might have been physical. Cells were injected after scaffold implantation, so the sponge was most probably not exerting any absorption of liquid, as they were already equilibrated with the liquids inside the cavity. By exclusion, this effect may be related to sponge stiffness, as stiffness gradients can induce cell migration [57,58]. Considering this, the young modulus of SF-HA-Hep sponges (13 KPa) [17] is larger than that of the human brain (1–10 KPa) [59,60], but may better suit the tumor microenvironment, where the altered ECM presents enhanced matrix stiffness (11.4 to 33.1 KPa) [61]. Thus, SF-HA-Hep sponges may confer to cells a suitable substrate with stronger mechanical forces than the brain ECM, allowing them to move upgradient, in a durotaxis response.

The reverse effect of the ECM on cancer cells and the progression of tumors remains to be investigated [28,29,62,63]. Here, we showed that alteration of the tumor ecosystem can be done by the implantation of SF-HA-Hep sponges in the resection cavity. The exact underlying mechanisms of how SF-HA-Hep sponges helped to the resection cavity siting and shaping of the tumors remain to

be completely determined. Further studies including scaffold-to-tumor distance variation, the measuring of mechano-sensing markers and the identification of immune cells can give more clarification in this matter. Overall, the biological and mechanical properties of SF-HA-Hep sponges may allow the concentration of remaining GB cells in a controllable area for further elimination.

4.2. Limits and perspectives

Incorporating dynamic biological information into scaffolds to match the *in vivo* environment of the native tissue has gained great appreciation [64]. However, this design can be a colossal challenge considering the complexity of the aberrant cues and signaling of cancer. The increasing understanding of the pre-metastatic niches and their roles in welcoming metastatic dissemination [65–67] has inspired scientists to create different strategies to trap migrating cancer cells [6,68–70]. In our exploration of SDF-1α as a bait to attract GB cells, we have encountered several challenges.

4.2.1. Release and control of SDF-1α into the brain parenchyma

We were previously able to observe the capacity of SF-HA-Hep sponges to integrate SDF-1α into their structure according to the loading methods used by simple dropping [17]. The distribution profile of the protein inside the sponge was visualized using SDF-1α coupled to AlexaFluor 647 thus demonstrating a radial concentration gradient from the center (where the drop was deposited) toward the edges of the sponges [17]. The ability of heparin to bind SDF-1α in polymer matrices is a proven fact thus facilitating the loading of chemokine [71,72]. Here, the SDF-1α retention capacity displayed by the SF-HA-Hep sponge correlates with the presence of AF 647-SDF-1α within the sponges in the brain parenchyma on day 7 of evaluation.

For strategies envisaging to attract cancer cells from a distant site, chemoattraction is an attractive strategy. The first challenge is related to the design of the scaffold to provide a releasing signal so that it creates a gradient, perdures and gets to the site of cancer cell residence. SF-HA-Hep sponges showed strong retention of SDF-1α. The initial burst of SDF-1α that occurred during the first day was about 4 % of the total load, quickly reaching a 5 % cumulative release plateau thereafter [17]. *In vitro*, this initial burst of SDF-1α was enough to chemoattract U87MG-CXCR4+ cells. Indeed, the calculated concentration in 30 µL of liquid within the well of the agarose gel (1070 ng/mL) was sufficient to create a gradient of SDF-1α. And, even if all the released SDF-1α were diffused within the 3-mL gel, the final concentration (10.7 ng/mL) would still be active [14]. Nevertheless, these remarks may not apply to the *in vivo* scenario. In this case, 32 ng of SDF-1α are released in a watery volume of ~20 µL corresponding to the resection cavity. Assuming a homogeneous distribution, the after-burst concentration of the soluble SDF-1α within the resection would be 1600 ng/mL. However, the surgical procedure involves leakage from drained liquids, including blood; therefore, it seems difficult that this concentration remains within the cavity. Moreover, if we consider SDF-1α degradation by enzymes and the inflammatory environment, the calculated SDF-1α initial concentration would be further reduced. In addition, SDF-1α being a small cytokine is rapidly dispersed in a water environment but the diffusion coefficient in the brain may be different.

Importantly, no AF647-SDF-1α was detected by fluorescence in the brain parenchyma, apart from the signal present in the detaching bulges from the edges of the sponges corresponding to the heparin complexed form of SDF-1α (Fig. 6A). Of note is that the levels of detection of the fluorescent protein by WB were only possible at 100 ng of protein concentrated in a band (Fig. 6B**).** Therefore, it is possible that lower levels of AF-647 were not detected in the brain parenchyma. Further studies need to consider different time points to evaluate the *in vivo* releasing profile of SDF-1α from the sponges using a radiolabeled protein. Discerning between chemotaxis and haptotaxis can be addressed by varying the placement of cells relative to sponges. Here, the effect of SDF-1α can be explained in part by a combination of chemotaxis and haptotaxis signaling as cells were injected beside the sponges. Under the premise that if SDF-1α is not released then chemoattraction can be limited, to improve the releasing profile of the chemokine, another strategy can be envisaged such as the incorporation of the protein into nanoparticles [73,74] for further integration into the sponges.

The optimal concentration of SDF-1α for GB-cell attraction may depend on several factors such as the stage of the disease, the type of cells involved, and the presence of other factors that may influence the chemokine activity. The effects of SDF-1α on cancer cell behavior can be concentration-dependent. Low concentrations of SDF-1α can promote cancer cell migration and invasion, while high concentrations can inhibit these processes by causing receptor internalization and desensitization [75]. Pasquier et al. (2015) showed that low concentrations of SDF-1α promote the migration of breast cancer cells through the activation of RhoA, while high concentrations increased adhesion through the activation of Rac1 [76]. Therefore, the task involves the design of a releasing profile to reach a steady state biological concentration of the chemokine during the time required to reach the target, which implies further and in-depth knowledge of the system.

4.2.2. Pleiotropic effects of SDF-1a

The concept of tumor entrapment aims to confine and eliminate cancer cells within a controlled microenvironment. Two primary strategies involve synergy with locoregional irradiation and the use of compounds to counteract tumor cell growth and resistance. SDF-1α, a versatile signaling molecule, plays a pivotal role in various biological processes. Its initial advantages, such as chemoattraction and migration, can turn detrimental to inhibiting proliferation. Hence, the development of diverse SDF-1α analogs offers promise for selectively modulating its functions [77]. Exploring distinct SDF-1 isoforms like SDF-1γ, with unique biomatrix binding properties, can further optimize the balance between beneficial chemotaxis and reduced proliferation [78].

The SDF-1α network is intrinsically connected with several genetic and molecular events in the tumor microenvironment [79], reflecting in tumor growth and cell invasion. CXCR4-mediated chemotaxis can be mediated by the activation of PI3 kinase (PI3K) by both G$\beta\gamma$ and Gα subunits of the activated G-protein coupled receptor. PI3K activation results in the phosphorylation of several focal adhesion components, paxillin among them [80]. Tyr118, the main residue of paxillin phosphorylation by focal adhesion kinase (FAK) was found here in gradual phosphorylated levels according to the increasing time of exposure to SDF-1α, suggesting a gradual formation of focal adhesions [22]. However, we also found activation of Akt and Erk. Independent activation of Akt and ERK1/2 by SDF-1α can support cell growth [81], and exert a positive effect on the survival of GB cells [14].

Therefore, although the initial strategy of using SDF-1α as a chemoattractant was coherent with the observed gradual increase in p-paxillin and the strong chemotactic *in-vitro* response, the utilization of SDF-1α to attract infiltrative GB cells *in vivo* entails a risk of tumor progression and dissemination that must be evaluated. Indeed, we found that the effect of SDF-1α on migration was independent of cell proliferation *in vitro*. However, the reduced cell hallo observed in the ADC-treated agarose drops (proliferation inhibited), also suggests a positive effect of SDF-1α on survival and/or proliferation. Moreover, the *in vivo* observations about the larger average tumor size and reduced median survival suggest that SDF-1α contained within the sponges may favor the devel-

opment of the tumors. Therefore, this may lead to an increase in tumor aggressiveness if not controlled.

A better understanding of SDF-1α pathways' activation after loading into SF-HA-Hep sponges might help to find an optimal condition. For instance, SDF-1α forms oligomers upon binding to free GAGs in brain ECM, which implies the regulation of chemokine function [78]. Whether chemoattraction alone can be activated in the SDF1α /CXCR4 axis is not known. However, evidence exists that the SDF-1γ isoform did not induce robust cell motility unless it was bound to heparin [53,82]. Then, a modification of the scaffold-chemokine interaction or the use of a different isoform might favor chemotaxis against proliferation or survival.

4.2.3. Tumor heterogeneity, the evolution of cancer cells and endogenous signals

SDF-1α has been shown to exert a chemoattractant effect *in vitro* on GB patient-derived cell lines expressing the CXCR4 receptor [14]. In addition, U87MG-CXCR4+ cells are infiltrative into the normal mouse brain parenchyma [18]. However, cell lines may not represent completely GB as a heterogeneous tumor. Even if the cell of origin might be a common neural stem cell or progenitor cell [83], the evolution of the tumoral cell content is dictated by the tumoral ecosystem, and different glioma stem cells with their progeny may be present [84]. Therefore, the expression of the CXCR4 receptor might be variable, reducing the targeting efficiency.

Furthermore, the expression of endogenous signals in the brain can represent competitional zones for cell attraction. For example, we observed SDF-1α expression in blood vessels, which are sites of GB cell migration. Macrophage migration inhibitory factor (MIF) can also bind to the CXCR4 receptor, and it is expressed by U87MG cells (**Fig. S5**), therefore the autologous/paracrine signaling from the tumor itself can also interfere with the efficiency of the chemoattraction strategy.

4.2.4. Cellular/tissue barriers to migration

Another consideration is related to the body's reaction to the material itself. Fibrotic capsules are often formed in materials recognized as strange bodies as implanted devices [85]. The cellular and tissue barriers formed around them, represent then an obstacle to cell colonization. For example, the M-Trap device showed increased mean survival of human ovarian cancer xenografted rats [6], but has failed to demonstrate safety and efficacy in clinical trials. This was attributed to surgical complexity and the numerous intraperitoneal adhesions developed after implantation, preventing tumor cells from reaching the devices [86]. In the brain context, Autier et al. (2019), designed bacterial cellulose (BC) membranes for tumor bed implantation, as a system for trapping residual GB cells. *In vitro* assessments showed that F98 tumor cells were trapped and unable to move onto the surface of the membranes. However, a fibrous capsule was observed around the material after brain implantation, which may prevent or decrease cell access [87]. This reaction was not observed for any of the implanted sponges as demonstrated by the histological analysis in rats, however the host reaction might be different as observed in humans for the M-trap device.

4.2.5. Tumor microenvironment (TME)'s response

SF-HA-Hep sponges caused an acute and chronic inflammatory response that was characteristic of a foreign body reaction with the recruitment of PMN cells, macrophages and lymphocytes. The presence of diverse cell types within the GB TME can influence the progression of the disease. For instance, GB cells are thought to induce an immunosuppressive environment by secretion of different factors. Among them, M-CSF, TGFb-1 and IL-10 skew macrophages to the immunosuppressive M2 phenotype [88]. The presence of M2-stage macrophages is correlated with vessel dilation and malignancy in different human glioma samples [89]. Furthermore, normal monocytes exposed to glioma cells acquire properties like those of myeloid-derived suppressor cells (MDSCs) [90]. Secretion of VEGF induces neoangiogenesis, inhibits maturation of dendritic cells, hinders infiltration of effector T-cells and activates antigen-specific regulatory T cells [91]. In addition, reactive astrogliosis produces growth factors, cytokines and metabolites that promote gliomagenesis [92]. We observed the presence of PMN cells and chronic inflammatory cells in both SF-HA-Hep and control cavities without sponges. Although this observation was true in the immunocompetent Fischer rats, nude rats (with 70 % Fischer background, Janvier Labs) may have a similar response due to the presence of most of these immune cells except for mature T-cells. In nude animals, SF-HA-Hep implantation alone did not influence survival as compared to cavities, therefore the discrimination of a positive effect of the inflammatory response on tumor progression cannot be discerned. To explore the effect of the whole immune system, the complete immunocompetent model would have to be used. Whether these immune reactions could be exploited for targeting cancer cells remains to be explored, i.e., the reversion into a positive factor for GB treatment.

Taken together, these listed factors should be considered in the design of a tumor cell trapping strategy, independently of the molecules used. Their adequate consideration may increase the efficacy of the cell trapping capacity.

4.3. The resection cavity as a part of the pathology and perspectives on sponges as "meeting rooms" to direct the GB ecosystem

In operable GB, the resection cavity is part of the pathology. After tumor surgical resection, the brain parenchyma is extremely fragile, and the cavities present unpredictable shapes and sizes. These aspects hinder the local administration of post-operative treatments, resulting in a high probability of recurrence (~90 % of the cases) [93]. Mainly, tumor cells present in the peritumoral brain zone are responsible for that, and today it is impossible to image and target them using the maximum tolerated dose of radiotherapy after surgery [87]. However, the resection space can also offer an opportunity for the treatment of recurrent GB. The two main limitations contributing to the failure of conventional therapy are i) treatment resistance and ii) sub-optimal delivery of active principles. Different strategies have been investigated for the local and enhanced delivery of chemotherapeutic agents. Convection-enhanced delivery (CED) allows direct delivery of chemotherapeutics via a catheter in the tissue surrounding the GB resection cavity, but this method results in unpredictable brain diffusion and requires the use of several surgical procedures, leading to a high risk of infection or bleeding [94]. Other strategies include the use of hydrogels and other implantable scaffolds [95,96] for the sustained and local delivery of chemotherapeutics. However, only Gliadel wafers, consisting of an implantable copolymer that allows the controlled release of carmustine within the cavity, have reached the clinic. Recently, it was reported that adjuvant treatment with Gliadel may prolong the overall survival of malignant glioma patients [97], but their association with a high rate of complications is still controversial [98–100].

Alteration of the GB ecosystem may offer a new perspective for the targeting of the residual disease. Luring of GB cells is now being explored to concentrate GB cells for further elimination [7,87]. For this purpose, the use of an implantable support as means of direct contact with the brain parenchyma is fundamental for the targeting of residual GB cells. In this line, shape-memory lasting SF-HA-Hep sponges may allow the brain parenchyma to have better structural support, preventing a collapse of this tissue after surgery and lasting long enough to permit cell infiltration.

However, the limitations presented and discussed for the tumor cell trapping strategy may still impede the complete eradication of infiltrative GB cells. Combined approaches, such as the use of chemoattractants and killing agents [101], local radiotherapy [18], or the delivery of cellular components such as engineered tumoricidal neural stem cells [102] may help a better outcome.

Switching the focus from the cancer cell alone to one that includes the normal host environment offers new perspectives [28,103]. SF-HA-Hep sponges and other implants [6,87] caused a local inflammatory response. Moreover, the presence of CD11b/c-positive cells inside the sponges and GFAP-positive cells in the vicinity of the cavities seven days post-implantation (**Supp. Fig. 6**) indicate that various cell types can interact with the implant, regardless of whether it is loaded with SDF-1α or not. These interactions could potentially impact the TME. Integrin CD11b is primarily expressed in monocytes, macrophages, neutrophils, dendritic cells (DCs), NK cells, and a subset of B and T cells (absent in the case of nude rats). Conversely, CD11c is a widely used marker for defining DCs [104] . The Glial fibrillary acidic protein (GFAP), on the other hand, is specifically found in the astroglial cytoskeleton [105]. Ideally, implantable materials should have a regenerating anti-inflammatory and neuro-regenerative effect after surgical resection of the tumor [28,106]. However, the inflammatory cells observed in the cavities might be reeducated for the tackling of tumor cells. GB is known to create an immunosuppressive environment [107]. This is due to the crosstalk between glioma and immune cells, which opens the possibility of the immunomodulation of the TME. Therefore, the presence of macrophages and lymphocytes after implantation of SF-HA-Hep sponges could be reverted in a positive factor to improve the immune response against the tumor by loading other chemokines and immunostimulatory molecules. Additionally, the chronic inflammatory cells can help to break down the ECM and increase blood flow to the tumor, improving drug penetration and increasing treatment efficacy [108]. Further research is needed to fully understand the potential benefits of this approach as a “cell meeting room” implantable scaffold to remodel the GB ecosystem for better therapy outcomes.

5. Conclusion

The plethora of strategies investigated for GB treatment is impressive, but the reflection on patient survival is nowadays limited. This is due to the high infiltrative capacity of GB cells. Considering GB as an ecosystem disease may help in the designing of therapeutic strategies that explore the alteration of its elements such as migratory niches. Here, SF-HA-Hep sponges were able to attract GB cells from the parenchyma surrounding the created brain cavity in rats, and sited and shaped the tumors in the resection spaces. Besides, the sponges demonstrated to have characteristics compatible with an implantable biomaterial, adequate for the brain tissue. This work has shown this scaffold is a potential tool for GB treatment, although there are yet some limitations regarding the use of SDF-1α. The concentration of GB cells and the shaping of the tumor may improve cancer treatment by improving post-surgical outcomes, enhancing the effectiveness of chemotherapy and other targeted therapies, and improving the precision of radiation therapy. Still, limitations exist for the complete attraction of residual cells, therefore other combinatorial and immune-modulating approaches can be considered.

Data availability

The data that support the findings of this study are available from the corresponding authors, upon reasonable request.

Declaration of Competing Interest

The authors declare that they have no known competing financial interests or personal relationships that could have appeared to influence the work reported in this paper.

Acknowledgements

For critical platform assistance in developing this work, authors would like to thank Romain Mallet, Florence Manero and Rodolphe Perrot from SCIAM (Common Service for Imaging and Microscopy Analysis, SFR ICAT 4208, Université d’Angers, France), Florence Franconi and Samuel Bonnet from PRISM (Imagerie et spectroscopie multi-modales, SFR ICAT 4208, Université d’Angers, France), Catherine Guillet, Jérôme Cayon and Lydie Bonneau from PACeM (Plateforme d’Analyses Cellules et Moléculaire, SFR ICAT 4208, Université d’Angers, France), and Aurélia Rolland from IMAC (Imagerie Cellulaire, INRAE, Angers, France).The authors are also grateful to Luis Diaz-Gomez from USC (Universidade de Santiago de Compostela, Spain) for help with microCT analysis andLaurence Sindji and Anne Clavreul from CRCI2NA, team 5 GLIAD (Design and application of innovative local treatments in glioblastoma, Angers, France) for their useful advices.

Funding

This work was funded by the French National Research Agency (ANR) under the frame of EuroNanoMed III (project GLIOSILK “Silk-fibroin interventional nano-trap for the treatment of glioblastoma”) [grant ANR-19-ENM3-0003-01]. It was also supported by the Instituto de Salud Carlos III (ISCIII) [AC19/00067] Cofinanciado FEDER, Spain, by the Italian Ministry of Health-Ricerca Corrente Annual Program 2023, by the Institut National de la Santé et de la Recherche Médicale (INSERM) and by the University of Angers (Angers, France). The work was in addition related to: (i) to the French ANR under the frame of the LabEx IRON (Innovative Radiopharmaceuticals in Oncology and Neurology) as part of the French government Investissements d’Avenir program (ANR-11-LABX-0018 to E.G.); (ii) the “Région Pays-de-la-Loire” under the frame of the Target’In project (Improvement of targeting radiopharmaceuticals for better diagnostic and therapy in nuclear medicine to E.G.); iii) the “Ligue Nationale contre le Cancer” and the “Comité Départemental de Maine-et-Loire de la Ligue contre le Cancer” (CD49) under the frame of the FusTarG project (Design and application of precision RNA oligonucleotides and aptamers for targeting gene fusion products in glioblastoma to E.G.) and iv) the "Tumour targeting, Imaging and radiotherapies network" of the “Cancéropôle Grand-Ouest” (France). RMP was a PhD fellow from the French “Ministère de l’Enseignement supérieur, de la recherche et de l’innovation” (MESRI). MN received a PhD fellowship from “La Région Pays-de-la-Loire” under the frame of the Erasmus Mundus Joint Doctorate program for Nanomedicine and Pharmaceutical Innovation (EMJD NanoFar).

Supplementary materials

Supplementary material associated with this article can be found, in the online version, at doi:10.1016/j.actbio.2023.10.022.

References

[1] C. Birzu, P. French, M. Caccese, G. Cerretti, A. Idbaih, V. Zagonel, G. Lombardi, Recurrent glioblastoma: from molecular landscape to new treatment perspectives, Cancers 13 (2021) 47, doi:10.3390/cancers13010047.

[2] T. Yamahara, Y. Numa, T. Oishi, T. Kawaguchi, T. Seno, A. Asai, K. Kawamoto, Morphological and flow cytometric analysis of cell infiltration in glioblastoma: a comparison of autopsy brain and neuroimaging, Brain Tumor Pathol. 27 (2010) 81–87, doi:10.1007/s10014-010-0275-7.

[3] A. Giese, R. Bjerkvig, M.E. Berens, M. Westphal, Cost of migration: invasion of malignant gliomas and implications for treatment, J. Clin. Oncol. 21 (2003) 1624–1636, doi:10.1200/JCO.2003.05.063.
[4] M. Najberg, M. Haji Mansor, F. Boury, C. Alvarez-Lorenzo, E. Garcion, Reversing the tumor target: establishment of a tumor trap, Front. Pharmacol. 10 (2019) 887, doi:10.3389/fphar.2019.00887.
[5] B. Van Der Sanden, F. Appaix, F. Berger, L. Selek, J.-P. Issartel, D. Wion, Translation of the ecological trap concept to Glioma therapy: the cancer cell trap concept, Fut. Oncol. (2013) 817–824, doi:10.2217/fon.13.30.
[6] A. de la Fuente, L. Alonso-Alconada, C. Costa, J. Cueva, T. Garcia-Caballero, R. Lopez-Lopez, M. Abal, M-Trap: exosome-based capture of tumor cells as a new technology in peritoneal metastasis, J. Natl. Cancer Inst. (2015) 107, doi:10.1093/jnci/djv184.
[7] A. Jain, M. Betancur, G.D. Patel, C.M. Valmikinathan, V.J. Mukhatyar, A. Vakharia, S.B. Pai, B. Brahma, T.J. MacDonald, R.V. Bellamkonda, Guiding intracortical brain tumour cells to an extracortical cytotoxic hydrogel using aligned polymeric nanofibres, Nat. Mater. 13 (2014) 308–316, doi:10.1038/nmat3878.
[8] Y. Xu, C. Chen, P.B. Hellwarth, X. Bao, Biomaterials for stem cell engineering and biomanufacturing, Bioact. Mater. 4 (2019) 366–379, doi:10.1016/j.bioactmat.2019.11.002.
[9] A. Sood, A. Gupta, G. Agrawal, Recent advances in polysaccharides based biomaterials for drug delivery and tissue engineering applications, Carbohydr. Polym. Technol. Appl. 2 (2021) 100067, doi:10.1016/j.carpta.2021.100067.
[10] G. Jensen, J.L. Holloway, S.E. Stabenfeldt, Hyaluronic acid biomaterials for central nervous system regenerative medicine, Cells 9 (2020) 2113, doi:10.3390/cells9092113.
[11] J. Nicolas, S. Magli, L. Rabbachin, S. Sampaolesi, F. Nicotra, L. Russo, 3D Extracellular matrix mimics: fundamental concepts and role of materials chemistry to influence stem cell fate, Biomacromolecules 21 (2020) 1968–1994, doi:10.1021/acs.biomac.0c00045.
[12] M. Ehtesham, J.A. Winston, P. Kabos, R.C. Thompson, CXCR4 expression mediates glioma cell invasiveness, Oncogene 25 (2006) 2801–2806, doi:10.1038/sj.onc.1209302.
[13] D. Zagzag, M. Esencay, O. Mendez, H. Yee, I. Smirnova, Y. Huang, L. Chiriboga, E. Lukyanov, M. Liu, E.W. Newcomb, Hypoxia- and vascular endothelial growth factor-induced stromal cell-derived factor-1alpha/CXCR4 expression in glioblastomas: one plausible explanation of Scherer's structures, Am. J. Pathol. 173 (2008) 545–560, doi:10.2353/ajpath.2008.071197.
[14] Y. Zhou, P.H. Larsen, C. Hao, V.W. Yong, CXCR4 is a major chemokine receptor on Glioma cells and mediates their survival, J. Biol. Chem. 277 (2002) 49481–49487, doi:10.1074/jbc.M206222200.
[15] V.V.V. Hira, U. Verbovšek, B. Breznik, M. Srdič, M. Novinec, H. Kakar, J. Wormer, B.V. der Swaan, B. Lenarčič, L. Juliano, S. Mehta, C.J.F. Van Noorden, T.T. Lah, Cathepsin K cleavage of SDF-1α inhibits its chemotactic activity towards glioblastoma stem-like cells, Biochim. Biophys. Acta. Mol. Cell Res. 1864 (2017) 594–603, doi:10.1016/j.bbamcr.2016.12.021.
[16] H. Kim, H.S. Roh, J.E. Kim, S.D. Park, W.H. Park, J.-Y. Moon, Compound K attenuates stromal cell-derived growth factor 1 (SDF-1)-induced migration of C6 glioma cells, Nutr. Res. Pract. 10 (2016) 259–264, doi:10.4162/nrp.2016.10.3.259.
[17] M. Najberg, M. Haji Mansor, T. Taillé, C. Bouré, R. Molina-Peña, F. Boury, J.L. Cenis, E. Garcion, C. Alvarez-Lorenzo, Aerogel sponges of silk fibroin, hyaluronic acid and heparin for soft tissue engineering: composition-properties relationship, Carbohydr. Polym. 237 (2020) 116107, doi:10.1016/j.carbpol.2020.116107.
[18] D. Séhédic, I. Chourpa, C. Tétaud, A. Griveau, C. Loussouarn, S. Avril, C. Legendre, N. Lepareur, D. Wion, F. Hindré, F. Davodeau, E. Garcion, Locoregional confinement and major clinical benefit of 188Re-loaded CXCR4-targeted nanocarriers in an orthotopic human to mouse model of glioblastoma, Theranostics 7 (2017) 4517–4536, doi:10.7150/thno.19403.
[19] R. Milner, G. Edwards, C. Streuli, C. Ffrench-Constant, A role in migration for the alpha V beta 1 integrin expressed on oligodendrocyte precursors, J. Neurosci. 16 (1996) 7240–7252.
[20] B. Heit, P. Kubes, Measuring chemotaxis and chemokinesis: the under-agarose cell migration assay, Science's STKE 2003 (2003) pl5–pl5, doi:10.1126/stke.2003.170.pl5.
[21] N. Ishii, D. Maier, A. Merlo, M. Tada, Y. Sawamura, A.-C. Diserens, E.G. Van Meir, Frequent co-alterations of TP53, p16/CDKN2A, p14ARF, PTEN tumor suppressor genes in human glioma cell lines, Brain Pathol. 9 (1999) 469–479, doi:10.1111/j.1750-3639.1999.tb00536.x.
[22] Y. Hu, J. Lu, X. Xu, J. Lyu, H. Zhang, Regulation of focal adhesion turnover in SDF-1α-stimulated migration of mesenchymal stem cells in neural differentiation, Sci. Rep. 7 (2017) 10013, doi:10.1038/s41598-017-09736-7.
[23] A. Sehgal, C. Keener, A.L. Boynton, J. Warrick, G.P. Murphy, CXCR-4, a chemokine receptor, is overexpressed in and required for proliferation of glioblastoma tumor cells, J. Surg. Oncol. 69 (1998) 99–104 2<99::aid−jso10>3.0.co;2-m., doi:10.1002/(sici)1096-9098(199810)69.
[24] S. Chatterjee, B. Behnam Azad, S. Nimmagadda, Chapter Two - The intricate role of CXCR4 in cancer, in: M.G. Pomper, P.B. Fisher (Eds.), Advances in Cancer Research, Academic Press, 2014, pp. 31–82, doi:10.1016/B978-0-12-411638-2.00002-1.
[25] B.M. Woerner, N.M. Warrington, A.L. Kung, A. Perry, J.B. Rubin, Widespread CXCR4 activation in astrocytomas revealed by phospho-CXCR4-specific antibodies, Cancer Res. 65 (2005) 11392–11399, doi:10.1158/0008-5472.CAN-05-0847.
[26] X. Bian, S. Yang, J. Chen, Y. Ping, X. Zhou, Q. Wang, X. Jiang, W. Gong, H. Xiao, L. Du, Z. Chen, W. Zhao, J. Shi, J.M. Wang, Preferential expression of chemokine receptor CXCR4 by highly malignant human gliomas and its association with poor patient survival, Neurosurgery 61 (2007) 570–579, doi:10.1227/01.NEU.0000290905.53685.A2.
[27] L. Cheng, Z. Huang, W. Zhou, Q. Wu, S. Donnola, J.K. Liu, X. Fang, A.E. Sloan, Y. Mao, J.D. Lathia, W. Min, R.E. McLendon, J.N. Rich, S. Bao, Glioblastoma stem cells generate vascular pericytes to support vessel function and tumor growth, Cell 153 (2013) 139–152, doi:10.1016/j.cell.2013.02.021.
[28] A. Belousov, S. Titov, N. Shved, M. Garbuz, G. Malykin, V. Gulaia, A. Kagansky, V. Kumeiko, The extracellular matrix and biocompatible materials in glioblastoma treatment, Front. Bioeng. Biotechnol. 7 (2019) https://www.frontiersin.org/articles/10.3389/fbioe.2019.00341. (Accessed 17 March 2023).
[29] D. Sood, M. Tang-Schomer, D. Pouli, C. Mizzoni, N. Raia, A. Tai, K. Arkun, J. Wu, L.D. Black, B. Scheffler, I. Georgakoudi, D.A. Steindler, D.L. Kaplan, 3D extracellular matrix microenvironment in bioengineered tissue models of primary pediatric and adult brain tumors, Nat. Commun. 10 (2019) 4529, doi:10.1038/s41467-019-12420-1.
[30] E. Mohiuddin, H. Wakimoto, Extracellular matrix in glioblastoma: opportunities for emerging therapeutic approaches, Am. J. Cancer Res. 11 (2021) 3742–3754.
[31] S.S. Rao, J. DeJesus, A.R. Short, J.J. Otero, A. Sarkar, J.O. Winter, Glioblastoma behaviors in three-dimensional collagen-hyaluronan composite hydrogels, ACS Appl. Mater. Interfaces 5 (2013) 9276–9284, doi:10.1021/am402097j.
[32] C. Wang, X. Tong, F. Yang, Bioengineered 3D brain tumor model to elucidate the effects of matrix stiffness on glioblastoma cell behavior using PEG-based hydrogels, Mol. Pharm. 11 (2014) 2115–2125, doi:10.1021/mp5000828.
[33] J.-W.E. Chen, S. Pedron, P. Shyu, Y. Hu, J.N. Sarkaria, B.A.C. Harley, Influence of hyaluronic acid transitions in tumor microenvironment on glioblastoma malignancy and invasive behavior, Front. Mater. 5 (2018) https://www.frontiersin.org/articles/10.3389/fmats.2018.00039. (Accessed 17 March 2023).
[34] M. Bartoš, T. Suchý, R. Foltán, Note on the use of different approaches to determine the pore sizes of tissue engineering scaffolds: what do we measure? Biomed. Eng. Online 17 (2018) 110, doi:10.1186/s12938-018-0543-z.
[35] M. Saif Ur Rahman, J. Wu, H. Chen, C. Sun, Y. Liu, S. Xu, Matrix mechanophysical factor: pore size governs the cell behavior in cancer, Adv. Phys. 8 (2023) 2153624, doi:10.1080/23746149.2022.2153624.
[36] K. Wolf, M. Te Lindert, M. Krause, S. Alexander, J. Te Riet, A.L. Willis, R.M. Hoffman, C.G. Figdor, S.J. Weiss, P. Friedl, Physical limits of cell migration: control by ECM space and nuclear deformation and tuning by proteolysis and traction force, J. Cell Biol. 201 (2013) 1069–1084, doi:10.1083/jcb.201210152.
[37] K. Polyak, R.A. Weinberg, Transitions between epithelial and mesenchymal states: acquisition of malignant and stem cell traits, Nat. Rev. Cancer 9 (2009) 265–273, doi:10.1038/nrc2620.
[38] P.P. Provenzano, D.R. Inman, K.W. Eliceiri, S.M. Trier, P.J. Keely, Contact guidance mediated three-dimensional cell migration is regulated by Rho/ROCK-dependent matrix reorganization, Biophys. J. 95 (2008) 5374–5384, doi:10.1529/biophysj.108.133116.
[39] C.D. Paul, P. Mistriotis, K. Konstantopoulos, Cancer cell motility: lessons from migration in confined spaces, Nat. Rev. Cancer 17 (2017) 131–140, doi:10.1038/nrc.2016.123.
[40] S.M. Azarin, J. Yi, R.M. Gower, B.A. Aguado, M.E. Sullivan, A.G. Goodman, E.J. Jiang, S.S. Rao, Y. Ren, S.L. Tucker, V. Backman, J.S. Jeruss, L.D. Shea, In vivo capture and label-free detection of early metastatic cells, Nat. Commun. 6 (2015) 8094, doi:10.1038/ncomms9094.
[41] S. Aznavoorian, M.L. Stracke, H. Krutzsch, E. Schiffmann, L.A. Liotta, Signal transduction for chemotaxis and haptotaxis by matrix molecules in tumor cells, J. Cell Biol. 110 (1990) 1427–1438, doi:10.1083/jcb.110.4.1427.
[42] Z. Fan, F. Zhang, T. Liu, B.Q. Zuo, Effect of hyaluronan molecular weight on structure and biocompatibility of silk fibroin/hyaluronan scaffolds, Int. J. Biol. Macromol. 65 (2014) 516–523, doi:10.1016/j.ijbiomac.2014.01.058.
[43] K.J. Wolf, P. Shukla, K. Springer, S. Lee, J.D. Coombes, C.J. Choy, S.J. Kenny, K. Xu, S. Kumar, A mode of cell adhesion and migration facilitated by CD44-dependent microtentacles, Proc. Natl. Acad. Sci. 117 (2020) 11432–11443, doi:10.1073/pnas.1914294117.
[44] C.B.N. Mendes de Aguiar, B. Lobão-Soares, M. Alvarez-Silva, A.G. Trentin, Glycosaminoglycans modulate C6 glioma cell adhesion to extracellular matrix components and alter cell proliferation and cell migration, BMC Cell Biol. 6 (2005) 31, doi:10.1186/1471-2121-6-31.
[45] W.I. Choi, A. Sahu, C. Vilos, N. Kamaly, S.-M. Jo, J.H. Lee, G. Tae, Bioinspired heparin nanosponge prepared by photo-crosslinking for controlled release of growth factors, Sci. Rep. 7 (2017) 14351, doi:10.1038/s41598-017-14040-5.
[46] E.M. Rodrigues, A.L.G. Cornélio, P.H. Godoi, P.I. da Costa, C. Rossa-Junior, G. Faria, J.M. Guerreiro Tanomaru, M. Tanomaru-Filho, Heparin is biocompatible and can induce differentiation of human dental pulp cells, Int. Endod. J. 52 (2019) 829–837, doi:10.1111/iej.13061.
[47] B. Zhao, Z. Zhao, J. Ma, X. Ma, Modulation of angiogenic potential of tissue-engineered peripheral nerve by covalent incorporation of heparin and loading with vascular endothelial growth factor, Neurosci. Lett. 705 (2019) 259–264, doi:10.1016/j.neulet.2019.01.017.
[48] E.G. Hayman, M.D. Pierschbacher, S. Suzuki, E. Ruoslahti, Vitronectin–a major cell attachment-promoting protein in fetal bovine serum, Exp. Cell. Res. 160 (1985) 245–258, doi:10.1016/0014-4827(85)90173-9.
[49] X. Zhong, O. Arnolds, O. Krenczyk, J. Gajewski, S. Pütz, C. Herrmann, R. Stoll, The structure in solution of fibronectin type III domain 14 reveals its syner-

gistic heparin binding site, Biochemistry 57 (2018) 6045–6049, doi:10.1021/acs.biochem.8b00771.
[50] F.H. Seeger, T. Rasper, A. Fischer, M. Muhly-Reinholz, E. Hergenreider, D.M. Leistner, K. Sommer, Y. Manavski, R. Henschler, E. Chavakis, B. Assmus, A.M. Zeiher, S. Dimmeler, Heparin disrupts the CXCR4/SDF-1 axis and impairs the functional capacity of bone marrow–derived mononuclear cells used for cardiovascular repair, Circ. Res. 111 (2012) 854–862, doi:10.1161/CIRCRESAHA.112.265678.
[51] N. Rusetska, K. Kowalski, K. Zalewski, S. Zięba, M. Bidziński, K. Goryca, B. Kotowicz, M. Fuksiewicz, J. Kopczynski, E. Bakuła-Zalewska, A. Kowalik, M. Kowalewska, CXCR4/ACKR3/CXCL12 axis in the lymphatic metastasis of vulvar squamous cell carcinoma, J. Clin. Pathol. 75 (2022) 324–332, doi:10.1136/jclinpath-2020-206917.
[52] R. Janssens, A. Mortier, D. Boff, V. Vanheule, M. Gouwy, C. Franck, O. Larsen, M.M. Rosenkilde, J.V. Damme, F.A. Amaral, M.M. Teixeira, S. Struyf, P. Proost, Natural nitration of CXCL12 reduces its signaling capacity and chemotactic activity in vitro and abrogates intra-articular lymphocyte recruitment in vivo, Oncotarget 7 (2016) 62439–62459, doi:10.18632/oncotarget.11516.
[53] C. Laguri, R. Sadir, P. Rueda, F. Baleux, P. Gans, F. Arenzana-Seisdedos, H. Lortat-Jacob, The Novel CXCL12γ isoform encodes an unstructured cationic domain which regulates bioactivity and interaction with both glycosaminoglycans and CXCR4, PLoS One 2 (2007) e1110, doi:10.1371/journal.pone.0001110.
[54] K.M. Yamada, M. Sixt, Mechanisms of 3D cell migration, Nat. Rev. Mol. Cell Biol. 20 (2019) 738–752, doi:10.1038/s41580-019-0172-9.
[55] B.A. Aguado, R.M. Hartfield, G.G. Bushnell, J.T. Decker, S.M. Azarin, D. Nanavati, M.J. Schipma, S.S. Rao, R.S. Oakes, Y. Zhang, J.S. Jeruss, L.D. Shea, Biomaterial scaffolds as pre-metastatic niche mimics systemically alter the primary tumor and tumor microenvironment, Adv. Healthc. Mater. 7 (2018) 1700903, doi:10.1002/adhm.201700903.
[56] E. Nakayama, Y. Shiratsuchi, Y. Kobayashi, K. Nagata, The importance of infiltrating neutrophils in SDF-1 production leading to regeneration of the thymus after whole-body X-irradiation, Cell. Immunol. 268 (2011) 24–28, doi:10.1016/j.cellimm.2011.01.006.
[57] K.M. Yamada, J.W. Collins, D.A. Cruz Walma, A.D. Doyle, S.G. Morales, J. Lu, K. Matsumoto, S.S. Nazari, R. Sekiguchi, Y. Shinsato, S. Wang, Extracellular matrix dynamics in cell migration, invasion and tissue morphogenesis, Int. J. Exp. Pathol. 100 (2019) 144–152, doi:10.1111/iep.12329.
[58] J.A. Davies, Chapter 11 - Guidance by contact, in: J.A. Davies (Ed.), Mechanisms of Morphogenesis (Second Edition), Academic Press, Boston, 2013, pp. 129–145, doi:10.1016/B978-0-12-391062-2.00011-5.
[59] M.M. Nava, M.T. Raimondi, R. Pietrabissa, Controlling self-renewal and differentiation of stem cells via mechanical cues, Biomed. Res. Int. 2012 (2012) e797410, doi:10.1155/2012/797410.
[60] G. Singh, A. Chanda, Mechanical properties of whole-body soft human tissues: a review, Biomed. Mater. 16 (2021), doi:10.1088/1748-605X/ac2b7a.
[61] Y. Peng, Z. Chen, Y. He, P. Li, Y. Chen, X. Chen, Y. Jiang, X. Qin, S. Li, T. Li, C. Wu, H. Yang, F. You, Y. Liu, Non-muscle myosin II isoforms orchestrate substrate stiffness sensing to promote cancer cell contractility and migration, Cancer Lett. 524 (2022) 245–258, doi:10.1016/j.canlet.2021.10.030.
[62] A.E. Erickson, S.K. Lan Levengood, J. Sun, F.-C. Chang, M. Zhang, Fabrication and characterization of chitosan–hyaluronic acid scaffolds with varying stiffness for glioblastoma cell culture, Adv. Healthc. Mater. 7 (2018) 1800295, doi:10.1002/adhm.201800295.
[63] A. Saleh, E. Marhuenda, C. Fabre, Z. Hassani, J. de Weille, H. Boukhaddaoui, S. Guelfi, I.L. Maldonado, J.-P. Hugnot, H. Duffau, L. Bauchet, D. Cornu, N. Bakalara, A novel 3D nanofibre scaffold conserves the plasticity of glioblastoma stem cell invasion by regulating galectin-3 and integrin-β1 expression, Sci. Rep. 9 (2019) 14612, doi:10.1038/s41598-019-51108-w.
[64] J. Litowczenko, M.J. Woźniak-Budych, K. Staszak, K. Wieszczycka, S. Jurga, B. Tylkowski, Milestones and current achievements in development of multifunctional bioscaffolds for medical application, Bioact. Mater. 6 (2021) 2412–2438, doi:10.1016/j.bioactmat.2021.01.007.
[65] B.A. Aguado, G.G. Bushnell, S.S. Rao, J.S. Jeruss, L.D. Shea, Engineering the pre-metastatic niche, Nat. Biomed. Eng. 1 (2017) 0077, doi:10.1038/s41551-017-0077.
[66] G. Bassi, S. Panseri, S.M. Dozio, M. Sandri, E. Campodoni, M. Dapporto, S. Sprio, A. Tampieri, M. Montesi, Scaffold-based 3D cellular models mimicking the heterogeneity of osteosarcoma stem cell niche, Sci. Rep. 10 (2020) 22294, doi:10.1038/s41598-020-79448-y.
[67] E. D'Angelo, D. Natarajan, F. Sensi, O. Ajayi, M. Fassan, E. Mammano, P. Pilati, P. Pavan, S. Bresolin, M. Preziosi, R. Miquel, Y. Zen, S. Chokshi, K. Menon, N. Heaton, G. Spolverato, M. Piccoli, R. Williams, L. Urbani, M. Agostini, Patient-derived scaffolds of colorectal cancer metastases as an organotypic 3D model of the liver metastatic microenvironment, Cancers 12 (2020) 364, doi:10.3390/cancers12020364.
[68] Y. Huang, A. Hakamivala, S. Li, A. Nair, R. Saxena, J.-T. Hsieh, L. Tang, Chemokine releasing particle implants for trapping circulating prostate cancer cells, Sci. Rep. 10 (2020) 4433, doi:10.1038/s41598-020-60696-x.
[69] R.S. Oakes, G.G. Bushnell, S.M. Orbach, P. Kandagatla, Y. Zhang, A.H. Morris, M.S. Hall, P. LaFaire, J.T. Decker, R.M. Hartfield, M.D. Brooks, M.S. Wicha, J.S. Jeruss, L.D. Shea, Metastatic conditioning of myeloid cells at a subcutaneous synthetic niche reflects disease progression and predicts therapeutic outcomes, Cancer Res. 80 (2020) 602–612, doi:10.1158/0008-5472.CAN-19-1932.
[70] Q. Xiong, N. Zhang, M. Zhang, M. Wang, L. Wang, Y. Fan, C.-Y. Lin, Engineer a pre-metastatic niched microenvironment to attract breast cancer cells by utilizing a 3D printed polycaprolactone/nano-hydroxyapatite osteogenic scaffold – an in vitro model system for proof of concept, J. Biomedic. Mater. Res. Part B 110 (2022) 1604–1614, doi:10.1002/jbm.b.35021.
[71] M.S. Krieger, J.M. Moreau, H. Zhang, M. Chien, J.L. Zehnder, M.A. Nowak, M. Craig, Novel cytokine interactions identified during perturbed hematopoiesis, (2018) 484170. https://doi.org/10.1101/484170.
[72] S. Prokoph, E. Chavakis, K.R. Levental, A. Zieris, U. Freudenberg, S. Dimmeler, C. Werner, Sustained delivery of SDF-1α from heparin-based hydrogels to attract circulating pro-angiogenic cells, Biomaterials 33 (2012) 4792–4800, doi:10.1016/j.biomaterials.2012.03.039.
[73] R. Molina-Peña, M. Haji Mansor, M. Najberg, J.-M. Thomassin, B. Gueza, C. Alvarez-Lorenzo, E. Garcion, C. Jérôme, F. Boury, Nanoparticle-containing electrospun nanofibrous scaffolds for sustained release of SDF-1α, Int. J. Pharm. 610 (2021) 121205, doi:10.1016/j.ijpharm.2021.121205.
[74] S. Gascon, A. Giraldo Solano, W. El Kheir, H. Therriault, P. Berthelin, B. Cattier, B. Marcos, N. Virgilio, B. Paquette, N. Faucheux, M.-A. Lauzon, Characterization and mathematical modeling of alginate/chitosan-based nanoparticles releasing the chemokine CXCL12 to attract glioblastoma cells, Pharmaceutics 12 (2020) 356, doi:10.3390/pharmaceutics12040356.
[75] S. Tavor, I. Petit, S. Porozov, A. Avigdor, A. Dar, L. Leider-Trejo, N. Shemtov, V. Deutsch, E. Naparstek, A. Nagler, T. Lapidot, CXCR4 regulates migration and development of human acute myelogenous leukemia stem cells in transplanted NOD/SCID mice, Cancer Res. 64 (2004) 2817–2824, doi:10.1158/0008-5472.CAN-03-3693.
[76] J. Pasquier, N. Abu-Kaoud, H. Abdesselem, A. Madani, J. Hoarau-Véchot, H.Al. Thawadi, F. Vidal, B. Couderc, G. Favre, A. Rafii, SDF-1alpha concentration dependent modulation of RhoA and Rac1 modifies breast cancer and stromal cells interaction, BMC Cancer 15 (2015) 569, doi:10.1186/s12885-015-1556-7.
[77] A. Faber, C. Roderburg, F. Wein, R. Saffrich, A. Seckinger, K. Horsch, A. Diehlmann, D. Wong, G. Bridger, V. Eckstein, A.D. Ho, W. Wagner, The many facets of SDF-1alpha, CXCR4 agonists and antagonists on hematopoietic progenitor cells, J. Biomed. Biotechnol. 2007 (2007) 26065, doi:10.1155/2007/26065.
[78] E. Migliorini, D. Thakar, J. Kühnle, R. Sadir, D.P. Dyer, Y. Li, C. Sun, B.F. Volkman, T.M. Handel, L. Coche-Guerente, D.G. Fernig, H. Lortat-Jacob, R.P. Richter, Cytokines and growth factors cross-link Heparan sulfate, Open Biol. 5 (2015) 150046, doi:10.1098/rsob.150046.
[79] E. Henke, R. Nandigama, S. Ergün, Extracellular matrix in the tumor microenvironment and its impact on cancer therapy, Front Mol. Biosci. 6 (2020) https://www.frontiersin.org/articles/10.3389/fmolb.2019.00160. (Accessed 17 March 2023).
[80] B.A. Teicher, S.P. Fricker, CXCL12 (SDF-1)/CXCR4 pathway in cancer, Clinic. Cancer Res. 16 (2010) 2927–2931, doi:10.1158/1078-0432.CCR-09-2329.
[81] R. Würth, A. Bajetto, J.K. Harrison, F. Barbieri, T. Florio, CXCL12 modulation of CXCR4 and CXCR7 activity in human glioblastoma stem-like cells and regulation of the tumor microenvironment, Front. Cell Neurosci. 8 (2014) 144, doi:10.3389/fncel.2014.00144.
[82] M. Janowski, Functional diversity of SDF-1 splicing variants, Cell Adh. Migr. 3 (2009) 243–249, doi:10.4161/cam.3.3.8260.
[83] S.R. Alcantara Llaguno, L.F. Parada, Cell of origin of glioma: biological and clinical implications, Br. J. Cancer 115 (2016) 1445–1450, doi:10.1038/bjc.2016.354.
[84] O.O. Kanu, A. Mehta, C. Di, N. Lin, K. Bortoff, D.D. Bigner, H. Yan, D.C. Adamson, Glioblastoma multiforme: a review of therapeutic targets, Expert Opin. Ther. Targets 13 (2009) 701–718, doi:10.1517/14728220902942348.
[85] C. Horejs, Preventing fibrotic encapsulation, Nat. Rev. Mater. 6 (2021) 554, doi:10.1038/s41578-021-00338-4.
[86] A. Gil-Moreno, L. Alonso-Alconada, B. Díaz-Feijoo, S. Domingo, A. Vilar, A. Hernández, J. Gilabert, A. Llueca, A. Torné, J. de Santiago, M. Carbonell-Socias, V. Lago, E. Arias, V. Sampayo, J. Siegrist, A. Chipirliu, J.L. Sánchez-Iglesias, A. Pérez-Benavente, P. Padilla-Iserte, M. Santacana, X. Matias-Guiu, M. Abal, R. Lopez-Lopez, M-TRAP: safety and performance of metastatic tumor cell trap device in advanced ovarian cancer patients, Gynecol. Oncol. 161 (2021) 681–686, doi:10.1016/j.ygyno.2021.03.022.
[87] L. Autier, A. Clavreul, M.L. Cacicedo, F. Franconi, L. Sindji, A. Rousseau, R. Perrot, C.N. Montero-Menei, G.R. Castro, P. Menei, A new glioblastoma cell trap for implantation after surgical resection, Acta Biomater. 84 (2019) 268–279, doi:10.1016/j.actbio.2018.11.027.
[88] E.K. Nduom, M. Weller, A.B. Heimberger, Immunosuppressive mechanisms in glioblastoma, Neuro. Oncol. 17 (Suppl 7) (2015) vii9–vii14, doi:10.1093/neuonc/nov151.
[89] T. Mathivet, C. Bouleti, M. Van Woensel, F. Stanchi, T. Verschuere, L.-K. Phng, J. Dejaegher, M. Balcer, K. Matsumoto, P.B. Georgieva, J. Belmans, R. Sciot, C. Stockmann, M. Mazzone, S. De Vleeschouwer, H. Gerhardt, Dynamic stroma reorganization drives blood vessel dysmorphia during glioma growth, EMBO Mol. Med. 9 (2017) 1629–1645, doi:10.15252/emmm.201607445.
[90] J.C. Rodrigues, G.C. Gonzalez, L. Zhang, G. Ibrahim, J.J. Kelly, M.P. Gustafson, Y. Lin, A.B. Dietz, P.A. Forsyth, V.W. Yong, I.F. Parney, Normal human monocytes exposed to glioma cells acquire myeloid-derived suppressor cell-like properties, Neuro-oncology 12 (2010) 351–365, doi:10.1093/neuonc/nop023.
[91] G.T. Motz, G. Coukos, Deciphering and reversing tumor immune suppression, Immunity 39 (2013) 61–73, doi:10.1016/j.immuni.2013.07.005.

[92] S. De Vleeschouwer (Ed.), Glioblastoma, Codon Publications, Brisbane (AU), 2017 http://www.ncbi.nlm.nih.gov/books/NBK469998/ (Accessed 23 January 2023).
[93] J.-M. Lemée, A. Clavreul, P. Menei, Intratumoral heterogeneity in glioblastoma: don't forget the peritumoral brain zone, Neuro-oncology 17 (2015) 1322–1332, doi:10.1093/neuonc/nov119.
[94] E. Cruz Da Silva, M.-C. Mercier, N. Etienne-Selloum, M. Dontenwill, L. Choulier, A systematic review of glioblastoma-targeted therapies in phases II, III, IV clinical trials, Cancers 13 (2021) 1795, doi:10.3390/cancers13081795.
[95] C. Bastiancich, P. Danhier, V. Préat, F. Danhier, Anticancer drug-loaded hydrogels as drug delivery systems for the local treatment of glioblastoma, J. Controll. Release 243 (2016) 29–42, doi:10.1016/j.jconrel.2016.09.034.
[96] A. Djoudi, R. Molina-Peña, N. Ferreira, I. Ottonelli, G. Tosi, E. Garcion, F. Boury, Hyaluronic acid scaffolds for loco-regional therapy in nervous system related disorders, Int. J. Mol. Sci. 23 (2022) 12174, doi:10.3390/ijms232012174.
[97] T. Iuchi, A. Inoue, Y. Hirose, M. Morioka, K. Horiguchi, A. Natsume, Y. Arakawa, K. Iwasaki, M. Fujiki, T. Kumabe, Y. Sakata, Long-term effectiveness of Gliadel implant for malignant glioma and prognostic factors for survival: 3-year results of a postmarketing surveillance in Japan, Neuro-Oncol. Adv. 4 (2022) vdab189, doi:10.1093/noajnl/vdab189.
[98] C. Buonerba, G. Di Lorenzo, A. Marinelli, P. Federico, G. Palmieri, M. Imbimbo, P. Conti, G. Peluso, S. De Placido, J.H. Sampson, A comprehensive outlook on intracerebral therapy of malignant gliomas, Crit. Rev. Oncol. Hematol. 80 (2011) 54–68, doi:10.1016/j.critrevonc.2010.09.001.
[99] A. Bregy, A.H. Shah, M.V. Diaz, H.E. Pierce, P.L. Ames, D. Diaz, R.J. Komotar, The role of Gliadel wafers in the treatment of high-grade gliomas, Expert Rev. Anticancer Ther. 13 (2013) 1453–1461, doi:10.1586/14737140.2013.840090.
[100] E. Yeini, P. Ofek, N. Albeck, D. Rodriguez Ajamil, L. Neufeld, A. Eldar-Boock, R. Kleiner, D. Vaskovich, S. Koshrovski-Michael, S.I. Dangoor, A. Krivitsky, C. Burgos Luna, G. Shenbach-Koltin, M. Goldenfeld, O. Hadad, G. Tiram, R. Satchi-Fainaro, Targeting glioblastoma: advances in drug delivery and novel therapeutic approaches, Adv. Therap.. 4 (2021) 2000124. https://doi.org/10.1002/adtp.202000124.
[101] P.M. Kasapidou, E.L. de Montullé, K.-P. Dembélé, A. Mutel, L. Desrues, V. Gubala, H. Castel, Hyaluronic acid-based hydrogels loaded with chemoattractant and anticancer drug – new formulation for attracting and tackling glioma cells, Soft Matter 17 (2021) 10846–10861, doi:10.1039/D1SM01003D.
[102] K.T. Sheets, M.G. Ewend, M. Mohiti-Asli, S.A. Tuin, E.G. Loboa, K.S. Aboody, S.D. Hingtgen, Developing implantable scaffolds to enhance neural stem cell therapy for post-operative glioblastoma, Mol. Therapy 28 (2020) 1056–1067, doi:10.1016/j.ymthe.2020.02.008.
[103] A. De Boeck, B.Y. Ahn, C. D'Mello, X. Lun, S.V. Menon, M.M. Alshehri, F. Szulzewsky, Y. Shen, L. Khan, N.H. Dang, E. Reichardt, K.-A. Goring, J. King, C.J. Grisdale, N. Grinshtein, D. Hambardzumyan, K.M. Reilly, M.D. Blough, J.G. Cairncross, V.W. Yong, M.A. Marra, S.J.M. Jones, D.R. Kaplan, K.D. McCoy, E.C. Holland, P. Bose, J.A. Chan, S.M. Robbins, D.L. Senger, Glioma-derived IL-33 orchestrates an inflammatory brain tumor microenvironment that accelerates glioma progression, Nat. Commun. 11 (2020) 4997, doi:10.1038/s41467-020-18569-4.
[104] M. Gallizioli, F. Miró-Mur, A. Otxoa-de-Amezaga, R. Cugota, A. Salas-Perdomo, C. Justicia, V.H. Brait, F. Ruiz-Jaén, M. Arbaizar-Rovirosa, J. Pedragosa, E. Bonfill-Teixidor, M. Gelderblom, T. Magnus, E. Cano, C. Del Fresno, D. Sancho, A.M. Planas, Dendritic cells and microglia have non-redundant functions in the inflamed brain with protective effects of type 1 cDCs, Cell Rep. 33 (2020) 108291, doi:10.1016/j.celrep.2020.108291.
[105] Z. Yang, K.K.W. Wang, Glial fibrillary acidic protein: from intermediate filament assembly and gliosis to neurobiomarker, Trends Neurosci. 38 (2015) 364–374, doi:10.1016/j.tins.2015.04.003.
[106] B. Newland, P.B. Welzel, H. Newland, C. Renneberg, P. Kolar, M. Tsurkan, A. Rosser, U. Freudenberg, C. Werner, Tackling cell transplantation anoikis: an injectable, shape memory cryogel microcarrier platform material for stem cell and neuronal cell growth, Small 11 (2015) 5047–5053, doi:10.1002/smll.201500898.
[107] J.R.D. Pearson, S. Cuzzubbo, S. McArthur, L.G. Durrant, J. Adhikaree, C.J. Tinsley, A.G. Pockley, S.E.B. McArdle, Immune escape in glioblastoma multiforme and the adaptation of immunotherapies for treatment, Front. Immunol. 11 (2020) https://www.frontiersin.org/articles/10.3389/fimmu.2020.582106. (Accessed 17 March 2023).
[108] J. Huang, L. Zhang, D. Wan, L. Zhou, S. Zheng, S. Lin, Y. Qiao, Extracellular matrix and its therapeutic potential for cancer treatment, Sig. Transduct. Target Ther. 6 (2021) 1–24, doi:10.1038/s41392-021-00544-0.